Nonlinear stability and instability in collisionless trapped electron mode turbulence

D. A. Baver, P. W. Terry, and R. Gatto
University of Wisconsin-Madison, Madison, Wisconsin 53706

Eduardo Fernandez
Eckerd College, St. Petersburg, Florida 33711

(Received 23 January 2002; accepted 6 May 2002)

A two-field model for collisionless trapped electron mode turbulence has both finite amplitude-induced stability and instability, depending on wave number. Effects usually identified with nonlinear plasma instability (self-trapping, kinetics, 3D mode structure, magnetic shear) are absent. Nonlinear stability and instability reside in $E\times B$ advection of density. It drives modes of a purely damped branch of the dispersion relation to finite amplitude and changes the rate at which free energy is released into the turbulence by shifting the density-potential cross phase. Analysis shows that modes of the purely damped branch cannot be ignored in saturation, and that the linear growth rate is a poor indicator of driving at finite amplitude, invalidating mixing length and quasilinear approximations. Using statistical closure theory, the nonlinear eigenmode and growth rate are determined from the saturation level of modes on all branches, stable and unstable, and the nonlinear cross phase that governs finite-amplitude instability. © *2002 American Institute of Physics.* [DOI: 10.1063/1.1491958]

I. INTRODUCTION

Nonlinear instability is encountered in theoretical and numerical analyses of plasma turbulence with sufficient regularity[1–6] to warrant speculation that it is generic to plasma turbulence. A review of the literature suggests there is no universal process, but multiple mechanisms, including self-trapping,[1,2] kinetic effects,[1–3] 3D mode structure,[4,5] and magnetic shear.[5,6] Fluid descriptions of nonlinear instability have generally treated collisional regimes.[4–6] While subcritical instability is often examined, supercritical instability is also important, and easier to understand and analyze. In the latter, the rate at which energy is injected into the turbulence is not the linear growth rate. Hence, common turbulence characterizations that rely on the linear growth rate are invalidated.[7–9]

We demonstrate here the occurrence of both supercritical nonlinear instability and finite amplitude-induced stabilization of linearly unstable modes in the simplest type of plasma model for which nonlinear instability is possible, a two-field fluid model for 2D electrostatic turbulence in a homogeneous magnetic field.[10] Nonlinear instability is not possible in single-field models with energy-conserving nonlinearities; hence, the addition of a second dynamical equation represents the minimal increment in complexity allowing nonlinear instability. The present model is simpler than other systems in which nonlinear instability has been observed[1–6] because it lacks 3D mode structure, magnetic shear, kinetic effects, self-trapping in phase space, and collisional dynamics. The model provides a simple description of collisionless trapped electron turbulence, a fluctuation believed to contribute to anomalous transport in tokamaks. The simplicity of the model allows for detailed analysis of the nonlinear instability mechanism, which resides in the advection of electron density. Advection of scalars like density is intrinsic to many types of turbulence, suggesting that this mechanism is a player in more complicated types of turbulence, provided other effects do not negate it. Our model is similar to the Hasegawa–Wakatani equations.[11] The nonlinearities are identical, and in both models the linear coupling of density and potential is controlled by dissipation. When dissipation is strong the density is slaved to the potential, otherwise its evolution deviates from that of the potential. The dissipative coupling in the Hasegawa–Wakatani equation is nonlocal. Here, the magnetic field is treated as homogeneous, making the dissipative coupling local. This simplifies the system and its analysis. More importantly, the system is constrained by the removal of a degree of freedom, eliminating nonlinear instability mechanisms tied to mode structure and 3D effects.

Nonlinear instability is a reflection of the dynamical complexity intrinsic to two-field electrostatic turbulence, and demonstrates that generic one-field models cannot replicate the features of such turbulence. Because most measurements of turbulence in the core of tokamaks have been limited to a single type of fluctuation, generic single-field descriptions of electrostatic turbulence have been convenient for modeling and interpreting fluctuation data.[9] This work demonstrates that for collisionless plasmas such models are inadequate and misleading if used as a basis for interpreting diagnostic data. As such, it points to the need for diagnostic development to enable measurement of two fields, e.g., density and potential. This study also illustrates new physical processes that enter gyrokinetic simulations when nonadiabatic electrons are included.

The existence of supercritical instability and finite amplitude-induced stabilization has significant implications for the analytical treatment of saturation that use linear growth rates to approximate or calculate nonlinear quantities.

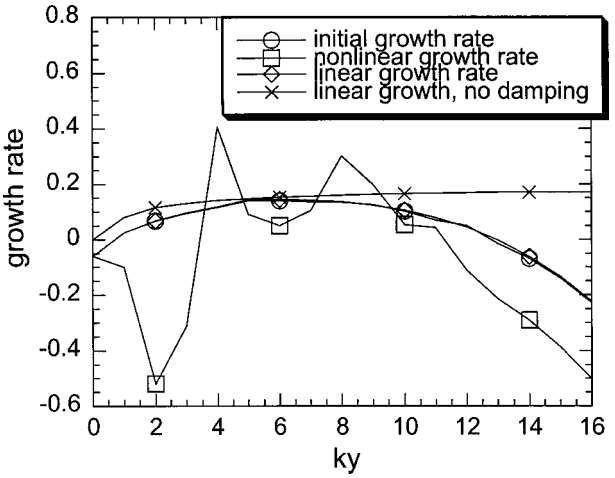

FIG. 1. Energy input rate as a function of k_y ($k_x=0$) at two times in the evolution of the system as compared to linear growth rates. The circles correspond to the exponential growth phase (infinitesimal amplitude) and the boxes to the saturated state (finite amplitude). The crosses indicate the model linear growth rate from Eq. (4), and the diamonds indicate the full linear growth rate with hyperviscous damping.

This type of treatment is common and forms the basis for mixing length estimates of turbulence levels, quasilinear estimates of transport fluxes,[7] estimates of E×B shearing thresholds using linear growth rates,[8] and indirect measurement of linear growth rates from fluctuation spectra using bispectral deconvolution.[9] We briefly touch on this issue by showing that for the present model there are significant differences between the quasilinear particle flux and the true nonlinear flux.

The nonlinear instability is depicted in Fig. 1, which is drawn from the numerical solutions more fully described in Sec. III. Two of the traces show spectra of the energy input rate at two times in the evolution of the system. The energy input rate is the rate at which energy is injected into the turbulence from the instability. The instability draws free energy from mean density and temperature gradients through dissipation. One trace (labeled with circles) is the rate during the linear growth phase, when fluctuation amplitudes are small and the nonlinearity is negligible. This rate agrees extremely well with the linear growth rate (diamonds), calculated from the unstable eigenmode of the linearized equations, as shown in Fig. 1. A second trace (boxes) is the energy input rate when the system has reached finite amplitude and the instability has saturated. The two traces (circles and diamonds) are markedly different. The difference is not the spectral energy transfer, which is conservative, but reflects a change in the dissipative process that extracts free energy from mean gradients and releases it into the turbulence. There is both nonlinear instability, evident in wave numbers for which the finite amplitude rate exceeds the linear rate, and finite amplitude-induced stabilization, evident in wave numbers for which the finite amplitude energy input rate is less than the linear growth rate.

We show that the difference between the energy input rate at infinitesimal and finite amplitudes originates with excitation of nonlinear eigenmode structure by the advective nonlinearity of electron density. The nonlinear eigenmode structure modifies the correlation between fluctuations of the electron density and the electrostatic potential, changing the rate at which free energy is released into the turbulence. Any fluctuation structure, including a nonlinear eigenmode, can be projected on the complete basis set of linear eigenmodes. Hence, the excitation of a nonlinear eigenmode that differs from the eigenmode of the linear instability necessarily implies that branches of the linear dispersion relation *for which all wave numbers are damped* are nonlinearly excited to finite amplitude. This is a standard concept in nonlinear systems analysis, yet such branches are routinely ignored in saturation analyses because it is assumed that linear damping makes the amplitudes of all Fourier modes negligible. In these analyses, saturation is achieved by nonlinear transfer of energy from unstable to stable Fourier modes *on the same branch* of the linear dispersion relation. This scenario essentially invokes a Kolmogorov cascade like that of Navier–Stokes turbulence. There is no nonlinear instability because stable modes of other branches are not included in saturation balances. We show here that the electron nonlinearity excites Fourier modes of the purely stable branch, provided the dynamics is collisionless. The excitation shifts the real frequency of the modes on this branch, and drives exponential growth, despite strong linear damping. At finite amplitude, modes of the purely stable branch change the correlation between density and potential, altering the energy injection rate. Moreover, because these modes are damped, their excitation to finite amplitude represents a significant energy dissipation channel that markedly alters saturation balances.

The physics of the nonlinear instability is analyzed using a general analytic theory that describes the nonlinear eigenmode and energy input rate. The basic equations are transformed to a diagonal representation of the linear coupling, and the finite-amplitude behavior of all branches of the linear dispersion relation is solved using an eddy-damped quasinormal Markovian (EDQNM) closure. The amplitudes of unstable Fourier modes are solved from the balance of the growth rate with nonlinear energy transfer, which now includes both spectral transfer to stable modes on the same branch and transfer to modes on the purely stable branch. The excitation level of modes on the purely stable branch is evaluated under a balance between nonlinear energy transfer to these modes and the damping rate of the branch. We show that this energy transfer is mediated by the complex-valued correlation between modes of each branch. The correlation must therefore be solved from its own spectrum balance equation obtained with the closure. The energies of modes on each branch and the cross correlation specify the complex-valued nonlinear eigenmode, and allow evaluation of density-potential cross correlation and the finite-amplitude energy input rate. We obtain the onset condition for excitation of modes on the purely stable branch, the finite amplitude-induced frequency and growth rate of these modes, the saturation levels of their energies, and the cross correlation of these modes with those of the unstable branch. All are in good agreement with numerical solutions. The complexities of the closure analysis make it impractical to evaluate the nonlinear growth rate analytically. However, we show that the phase of the cross correlation meets a neces-

sary condition for nonlinear instability, and that its magnitude is sufficient to produce the nonlinear growth rate spectrum of Fig. 1.

We stress that this method is very different from the more familiar nonlinear eigenmode analyses described in the literature.[12–14] These are generally based on a closure of amplitude equations in which the nonlinearities are transformed to diffusivities, and hence become dissipative. There is a nonlinear eigenmode at finite amplitude because the basic equations are approximated with a form that differs from that of the linear analysis. The modified form essentially alters the unstable branch, and does not involve stable branches of the eigenmode spectrum. These methods, which have been effective in describing changes to spatial structure of modes on the unstable branch at finite amplitude,[13,14] and have been applied to nonlinear instability in other systems,[12] fail to describe the nonlinear instability of the present model.

The remainder of the paper is organized as follows. In Sec. II the basic equations and their linear properties are presented, including linear eigenmode structure. Heuristic arguments demonstrating the role of electron density advection in the nonlinear instability and the excitation of the damped eigenmode are also presented. Section III presents a numerical description of the nonlinear instability and finite amplitude-induced stabilization process, showing the temporal evolution of modes on the unstable and stable branches, the nonlinear growth rate, and saturated spectra. Analytic treatment of the excitation of modes on the purely stable branch is given in Sec. IV, and the statistical closure theory in Sec. V. The closure equations are solved to obtain the energies of modes on the stable and unstable branches at saturation and the complex-valued cross correlation, thus specifying the nonlinear eigenmode. From it the energy input rate at finite amplitude is examined, and we show that supercritical instability in a band of linearly unstable modes is expected. Section VI presents conclusions and further discussion.

II. BASIC EQUATIONS AND LINEAR BEHAVIOR

The basic equations for the two-field trapped electron model represent a simple fluid system whose linear and nonlinear properties reproduce essential features of more complete descriptions. These features include instability in collisional and collisionless limits with real frequencies controlled by the electron diamagnetic frequency. They also include proper nonlinear dynamics, with long wavelength spectral energy transfer dominated by the E×B advection of electron density, and short wavelength transfer dominated by the ion polarization drift nonlinearity. In the collisionless limit, where the mode frequency of the instability ω exceeds the collision frequency υ, the growth rate is proportional to the small collision frequency. This is the only way to obtain instability in the absence of trapped particle resonances. The latter is the true source of instability in the collisionless limit; hence, the fluid instability is a surrogate. While the fluid instability is more correctly labeled as weakly collisional, the electron trapping regime, as delineated in kinetic theory, is said to be collisionless whenever $\omega > \upsilon$, even if υ is finite. It is in this sense that the dynamics studied herein is labeled as collisionless. The model is given by

$$\frac{\partial n}{\partial t} - \nabla\phi \times z \cdot \nabla n + \upsilon(n-\phi) = -\nu_D(1+\alpha\eta_e)\frac{\partial \phi}{\partial y}, \tag{1}$$

$$\frac{\partial}{\partial t}(1-\nabla^2-\varepsilon^{1/2})\phi - \varepsilon^{1/2}\upsilon(n-\phi) + \nabla\phi\times z\cdot\nabla\nabla^2\phi = -\nu_D[1-\varepsilon^{1/2}(1+\alpha\eta_e)]\frac{\partial\phi}{\partial y}, \tag{2}$$

where ϕ is the electrostatic potential, n is the density, $\varepsilon^{1/2}$ is the electron trapping fraction, $\upsilon = \upsilon_e/\varepsilon^{1/2}$ is the electron detrapping rate, υ_e is the electron collision rate, η_e is the ratio of the density gradient scale length to the temperature gradient scale length, $\nu_D = cT_e/eBL_n$ is the diamagnetic drift velocity, $L_n = (d\ln n_0/dx)^{-1}$ is the density gradient scale length, $\alpha = 3/2$, and the remaining symbols have their usual meaning. The density n is an effective electron density given by $n = \varepsilon^{-1/2}n_e + \phi$, where $n_e = \phi + \varepsilon^{1/2}\hat{n}_e$ is the usual electron density, consisting of the adiabatic contribution ϕ from passing electrons and the nonadiabatic contribution $\varepsilon^{1/2}\hat{n}_e$ from trapped electrons. In Eqs. (1)–(2), spatial scales are normalized to the ion gyroradius, evaluated at the electron temperature: $\rho_s = (\kappa T_e m_i)^{1/2}c/eB$, where m_i is the ion mass and κ is Boltzmann's constant. Temporal scales are normalized to ρ_s/C_s, where $C_s = (\kappa T_e/m_i)^{1/2}$ is the ion sound speed. The potential is normalized to $\kappa T_e/e$, and densities to the mean density. This system of equations has been studied in both the collisional[15,16] and collisionless limits.[10,17] In both limits, changes in the energy injection rate at finite amplitude have been reported.[10,16] The model is derived in the Appendix. In Eqs. (1)–(2) the linear coupling of the two fields is controlled by their difference and is mediated by the dissipation. For large collisionality, the adiabatic response, with $n \sim \phi$, is strongly enforced. In the collisionless limit the other terms, including the nonlinearity, enter the balance. An important aspect of the nonlinearity is finite amplitude-induced instability.

The evolution of the nonlinear instability and its eigenmode can be represented as an expansion in the complete basis set of linear eigenmodes. The model has two equations; hence, there are two linear eigenmode branches. One is the branch of the linear instability. It has exponentially growing fluctuations for certain wave numbers, and damped fluctuations at higher wave number. The other branch is stable for every Fourier wave number in the spectrum. The eigenfrequencies are given by the two branches of the quadratic dispersion relation

$$\omega^2(1+k^2-\varepsilon^{1/2}) + \omega[-\nu_D k_y(1-\varepsilon^{1/2}\hat{\alpha}) + i\upsilon(1+k^2)] - ik_y\nu_D\upsilon = 0, \tag{3}$$

where $\hat{\alpha} = 1 + \alpha\eta_e$. Restricting ourselves to the collisionless limit $\upsilon \ll \omega$, the frequency of the growing branch, through order $(\upsilon/k_y\nu_D)^2$, is

$$\omega=\omega_1=\frac{\nu_D k_y(1-\varepsilon^{1/2}\hat{\alpha})}{(1+k^2-\varepsilon^{1/2})}+\frac{i\upsilon\varepsilon^{1/2}[\hat{\alpha}(1+k^2)-1]}{(1+k^2-\varepsilon^{1/2})(1-\varepsilon^{1/2}\hat{\alpha})}+\frac{\upsilon^2\varepsilon^{1/2}[\hat{\alpha}(1+k^2)-1]}{k_y\nu_D(1-\varepsilon^{1/2}\hat{\alpha})^3}. \tag{4}$$

For instability, $\varepsilon^{1/2}\hat{\alpha}<1$. When a high k hyperviscous damping is added to Eq. (1), the imaginary part of Eq. (4), which gives the growth rate of the linear instability, takes the form shown in Fig. 1 for the infinitesimal energy input rate. The growth rate of Eq. (4) asymptotes to a constant positive value for large k; hence, the high-k damping in Fig. 1 comes entirely from the hyperviscosity. A small viscous damping rate at low k is also used in some simulations. Without low-k damping, ω_1 goes to zero for $k_y=0$. The eigenmode of the linear instability is an amplitude eigenvector, i.e., it specifies the relative amplitudes of n and ϕ under the instability. The eigenvector is obtained from either Eq. (1) or (2) by linearizing, Fourier transforming, substituting ω_1 for ω, and solving for n in terms of ϕ. The result is

$$n_k=\left[1+\frac{ik_y\nu_D(1-\varepsilon^{1/2}\hat{\alpha})-i\omega_1(1+k^2-\varepsilon^{1/2})}{\varepsilon^{1/2}\upsilon}\right]\phi_k=\left[\frac{\hat{\alpha}(1-\varepsilon^{1/2}+k^2)}{1-\varepsilon^{1/2}\hat{\alpha}}-\frac{i\upsilon[\hat{\alpha}(1+k^2)-1][1+k^2-\varepsilon^{1/2}]}{k_y\nu_D(1-\varepsilon^{1/2}\hat{\alpha})^3}+\mathrm{O}\left(\frac{\upsilon^2}{k_y^2\nu_D^2}\right)\right]\phi_k\equiv R_1(k)\phi_k. \tag{5}$$

Note that to lowest order, n and ϕ are of comparable magnitude and in phase.

The eigenmode of the nonlinear instability has, at finite amplitude, a non-negligible projection onto the branch of purely damped modes. Consequently, this branch cannot be ignored as is often done in analytic treatments. The frequency of the purely damped branch is

$$\omega=\omega_2=\frac{-i\upsilon}{(1-\varepsilon^{1/2}\hat{\alpha})}-\frac{\upsilon^2\varepsilon^{1/2}[\hat{\alpha}(1+k^2)-1]}{k_y\nu_D(1-\varepsilon^{1/2}\hat{\alpha})^3}+\mathrm{O}\left(\frac{\upsilon^3}{k_y^2\nu_D^2}\right), \tag{6}$$

and the eigenvector satisfies

$$n_k=\left[\frac{ik_y\nu_D(1-\varepsilon^{1/2}\hat{\alpha})}{\upsilon\varepsilon^{1/2}}+1-\frac{1+k^2-\varepsilon^{1/2}}{(1-\varepsilon^{1/2}\hat{\alpha})\varepsilon^{1/2}}+\frac{i\upsilon[\hat{\alpha}(1+k^2)-1](1+k^2-\varepsilon^{1/2})}{k_y\nu_D(1-\varepsilon^{1/2}\hat{\alpha})^3}+\mathrm{O}\left(\frac{\upsilon^2}{k_y^2\nu_D^2}\right)\right]\phi_k\equiv R_2(k)\phi_k. \tag{7}$$

This branch is damped for every wave number, even with no hyperviscosity. The damping rate is comparable in magnitude to the unstable branch growth rate. The purely damped branch differs from the unstable branch in three significant ways: (1) with $|R_2|=\mathrm{O}(k_y\nu_D/\upsilon)|R_1|$, its eigenvector has $n=\mathrm{O}(k_y\nu_D/\upsilon)\phi\gg\phi$; (2) to lowest order, its Fourier modes have zero real frequency; and (3) to lowest order, n is 90° out of phase with ϕ. The fact that $|R_2|\gg|R_1|$, and hence that $n\gg\phi$ for the damped branch, favors excitation of the damped branch by the electron nonlinearity. As shown in Sec. IV, the polarization drift nonlinearity drives the growing and damped branch amplitudes with forces of disparate magnitude. The damped branch force is smaller than the growing branch force by a factor $|R_1|/|R_2|=\mathrm{O}(\upsilon/k_y\nu_D)$. In contrast, the electron nonlinearity drives the damped branch with a force that is of equal magnitude to the force it exerts on the growing branch. Consequently, there is significant excitation of the damped branch in long-wavelength regimes where the electron nonlinearity dominates. In such regimes the spectrum reflects the partition of the purely damped branch, with n^2 becoming much greater than ϕ^2 as wave number increases.

Nonlinear excitation of the purely damped branch necessarily implies that the linear growth rate will change at finite amplitude. However, the change can be either positive or negative. To quantify the change in growth rate at finite amplitude, we introduce the energy input rate. For a system with conservative nonlinearities, this is proportional to the rate of change of total energy. It includes the energy fed into fluctuations at infinitesimal amplitude (linear growth rate) and at finite amplitude (nonlinear growth rate), and the energy removed from the system by dissipation. It does not include conservative processes such as spectral transfer. The energy is

$$W=\sum_k E(k)=\sum_k[(1+k^2-\varepsilon^{1/2})|\phi_k|^2+\varepsilon^{1/2}|n_k|^2]. \tag{8}$$

The rate of change of total energy is obtained from Eqs. (1)–(2) by taking the Fourier transform of each equation, multiplying Eq. (1) by ϕ_{-k} and Eq. (2) by $\varepsilon^{1/2}n_{-k}$, summing over wave number, and adding the two equations. The nonlinearities drop out of the resulting expression because they transfer energy in wave number space without energy loss, i.e., $\Sigma_k\Sigma_{k'}(\mathbf{k}'\times\mathbf{z}\cdot\mathbf{k})\ (k-k')^2\phi_{-k}\phi_{k'}\phi_{k-k'}=0$ and $\Sigma_k\Sigma_{k'}(\mathbf{k}'\times\mathbf{z}\cdot\mathbf{k})n_{-k}n_{k'}\phi_{k-k'}=0$. The rate of change of energy can be written

$$\frac{dW}{dt}=\sum_k 2\gamma_k^{nl}E(k), \tag{9}$$

where γ_k^{nl} is the energy input rate, given by

$$\gamma_k^{nl}=\frac{[k_y\nu_D\hat{\alpha}\varepsilon^{1/2}\,\mathrm{Im}\langle n_k^*\phi_k\rangle-\upsilon\varepsilon^{1/2}|(n_k-\phi_k)|^2]}{[(1+k^2-\varepsilon^{1/2})|\phi_k|^2+\varepsilon^{1/2}|n_k|^2]}. \tag{10}$$

Although the nonlinearities formally drop out of Eq. (9), γ_k^{nl} is fundamentally nonlinear. Only if n_k satisfies the eigenvector relation of the unstable branch [Eq. (7)] does Eq. (10) reproduce the linear growth rate. If n_k deviates from that relation, γ_k^{nl} deviates from the linear growth rate. Such a deviation occurs when the purely damped branch is excited nonlinearly. Instability, either linear or nonlinear, requires the first term of the numerator of γ_k^{nl} to be positive; the second term, which represents the dissipation from trapped electron scattering, is negative definite. The first term is driven by the free energy of the density and temperature gradients.

III. NUMERICAL SOLUTIONS

Equations (1) and (2) were solved numerically using a dealiased pseudospectral code. A hyperviscous damping was employed to provide dissipation at the highest wave numbers. Its magnitude is displayed in Fig. 1 as the difference between traces labeled with crosses [growth rate from Eq. (4)] and diamonds (growth rate with hyperviscous damping). At saturation the system is turbulent because, with a broad range of unstable modes, any given mode interacts simultaneously within multiple wave number triads, as evidenced by broad spectra in frequency and wave number. High resolution is not required, and runs typically had 33×33 modes. The mode $(k_x,k_y)=(0,0)$ does not evolve because its uniformity in all directions makes spatial derivatives vanish. Modes with $k_y=0$, $k_x\neq 0$, which include the zonally averaged flow and density, do evolve. The mean density appearing in L_n is taken as fixed, consistent with a steady state maintained by the balance of particle source and transport losses. The nonlinear instability is tied to fluctuation time scales and is not significantly affected by transport time-scale processes.

For a given set of parameters, the eigenmode relations of Eqs. (5) and (7) were calculated in the code. These were used to project the density and potential at each instant in time onto the complete basis set formed by the linear eigenmodes. The projection can be written

$$\begin{pmatrix} n_k(t) \\ \phi_k(t) \end{pmatrix} = \beta_1(k,t)\begin{pmatrix} R_1 \\ 1 \end{pmatrix} + \beta_2(k,t)\begin{pmatrix} R_2 \\ 1 \end{pmatrix} = \begin{pmatrix} R_1 & R_2 \\ 1 & 1 \end{pmatrix}\begin{pmatrix} \beta_1(k,t) \\ \beta_2(k,t) \end{pmatrix} \equiv \mathbf{M}\begin{pmatrix} \beta_1(k,t) \\ \beta_2(k,t) \end{pmatrix}, \tag{11}$$

where $\mathbf{M}$ is the matrix of the linear eigenvectors with elements R_1 and R_2 as defined in Eqs. (5) and (7), and β_1 and β_2 are the instantaneous amplitudes of the unstable and purely stable eigenmode branches, respectively. The instantaneous amplitude of each eigenmode evolves as the linearized normal mode in the linear phase, $\beta_j(k,t)=\beta_j(k,0)\exp(-i\omega_j t)$, and departs at finite amplitude. In the code, Eq. (11) is inverted at each instant in time to obtain the evolving eigenmode amplitudes as a function of the evolving density and potential.

Figure 2 shows time histories of the eigenmode energies W_{β_1} and W_{β_2}, and the total energy W. These energies are found from Eq. (8) by substituting Eq. (11) to obtain

$$W=\sum_k E(k)=W_{\beta_1}+W_{\beta_2}+\sum_k [(1+k^2-\varepsilon^{1/2}) \times 2\,\mathrm{Re}\langle\beta_1\beta_2^*\rangle+\varepsilon^{1/2}2\,\mathrm{Re}(R_1R_2^*\langle\beta_1\beta_2^*\rangle)], \tag{12}$$

where

$$W_{\beta_j}=\sum_k [(1+k^2-\varepsilon^{1/2})+\varepsilon^{1/2}|R_j|^2]|\beta_j|^2 \tag{13}$$

is the energy of the unstable ($j=1$) and purely stable ($j=2$) eigenmode branches. Note that because the linear eigenmode decomposition is nonorthogonal, the total energy

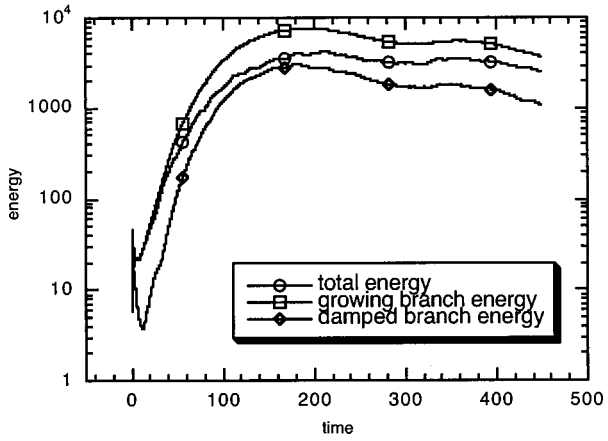

FIG. 2. The evolution of the energies of the growing linear eigenmode, damped linear eigenmode, and the total energy. The damped eigenmode decays initially but is then excited by the electron nonlinearity to a finite level.

is not simply the sum of the two eigenmode energies. There is an additional contribution involving $\langle\beta_1\beta_2^*\rangle$. These terms can be positive or negative. In Fig. 2 they are negative, and account for the fact that the total energy is smaller than W_{β_1}. More interesting is the behavior of W_{β_2}. The energy of the purely stable branch decays at the linear damping rate initially. However, shortly after $t=10$, the decay is suddenly arrested and the amplitude of the damped branch begins to grow exponentially. This continues until saturation, when both W_{β_1} and W_{β_2} reach a stationary, saturated level. In saturation, W_{β_2} is somewhat smaller than W_{β_1}. Because $|R_2|$ is larger than $|R_1|$ by a factor of order $k_y\nu_D/\nu$, β_1 is larger than β_2 by at least such a factor. For β_2, the phase of linear evolution occurs only for $t<10$, ending long before saturation and the termination of the linear growth phase of β_1.

The frequency spectrum of the damped branch $|\beta_2(k,\omega)|^2$ is constructed from a Fourier transform of $\beta_2(k,t)$ after saturation, and is displayed in Fig. 3. Spectra for β_1, n, ϕ are also displayed. During the linear growth phase we expect the spectrum to peak at $\omega=0$, consistent with Eq. (6), which indicates that the frequency of the damped eigenmode is zero up to order $(\nu/k_y\nu_D)^3$. In nonlinear regimes, frequency spectrum peaks are typically of order the linear frequency. However, Fig. 3 indicates that β_2 has a finite frequency of order $k_y\nu_D$. Thus, the process that excites β_2 to finite amplitude also gives it a significant nonzero frequency.

Wave number spectra for n and ϕ in the saturated state are given in Figs. 4(a) and (b). Both spectra peak at low wave number near $(k_x,k_y)=(0,1)$ and (1,0). In this region of wave number space, $|n_k|^2$ and $|\phi_k|^2$ are comparable. However, for high wave number, $|\phi_k|^2$ falls off much more rapidly than $|n_k|^2$. This can be attributed to the nonlinear advection of density, which in the collisionless regime excites the damped eigenmode with $n\gg\phi$. To test this hypothesis we obtained numerical solutions of Eqs. (1) and (2) for the *collisional regime*. In the collisional regime, $\nu\gg\omega$, $\nabla\phi\times z\cdot\nabla$, and Eq. (1) predicts an adiabatic electron response with $n\approx\phi$ to lowest order in $k_y\nu_D/\nu<1$. Indeed, the spectra of n

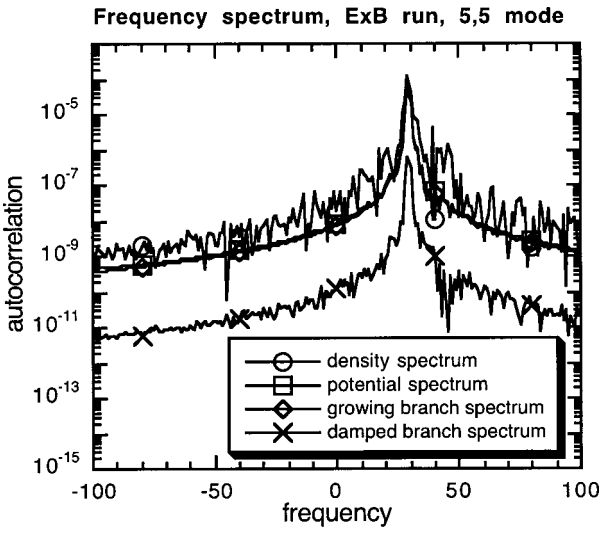

FIG. 3. Frequency spectrum at saturation of a Fourier mode of the purely stable eigenmode branch. The linear eigenfrequency is zero to lowest order. Nonlinearly, the mode has a frequency comparable to that of the unstable branch, i.e., comparable to $\nu_D k_y$.

and ϕ for the collisional regime satisfy $|n_k|^2 \approx |\phi_k|^2$ for all wave numbers, as evident in Figs. 5(a) and (b). Heavy ion beam probe measurements of both density and potential in the Texas Experimental Tokamak (TEXT) have recently been reported.[18] The density is comparable to the potential at low wave number, but falls off more gradually than the potential at high wave number. Qualitatively, the behavior is quite similar to that of Fig. 4. This comparison raises the possibility that nonlinear instability may have been present in the turbulence of TEXT. A method to infer the presence of nonlinear instability from the simultaneous measurement of density and potential[19] is currently under development for application to two-field data.

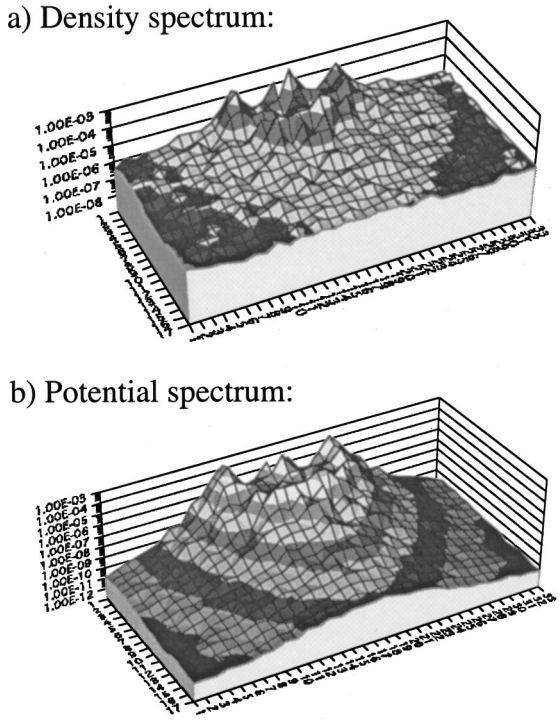

FIG. 4. Steady-state wave number spectra of (a) $|\phi_k|^2$ and (b) $|n_k|^2$.

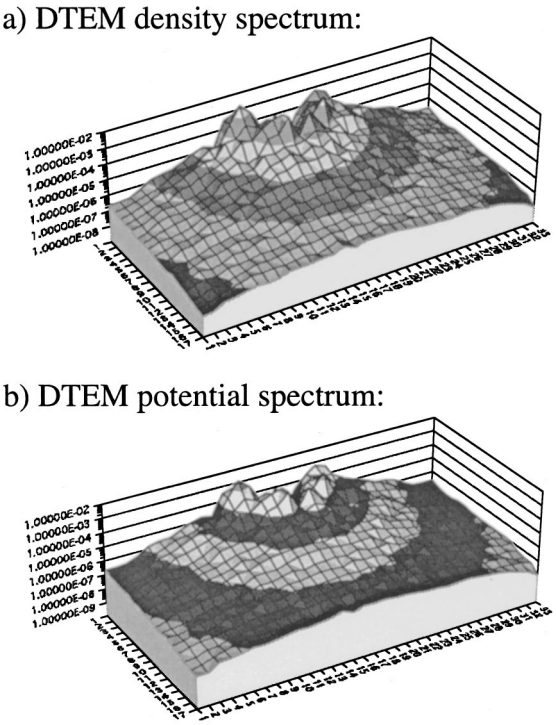

FIG. 5. Steady state wave number spectra for dissipative trapped electron mode turbulence for (a) $|\phi_k|^2$ and (b) $|n_k|^2$.

The behavior displayed in Fig. 2 and the spectra of Fig. 3 indicate a nonlinear eigenmode, and hence a nonlinear modification of the growth rate, either positive or negative. [Substitution of the unstable eigenmode density of Eq. (5) into Eq. (10) yields the linear growth rate; hence, any variation of n from the unstable eigenmode makes γ^{nl} different from the linear growth rate.] To determine the nonlinear growth rate we evaluate Eq. (10), taking $|n_k|^2$, $|\phi_k|^2$, and $\langle n_k^* \phi_k \rangle$ from temporal averages of simulation data in the saturated state. The result is Fig. 1, which was introduced in Sec. I. For this system there is supercritical instability at wave numbers around $k_y=4$ and $k_y=8$ (for $k_x=0$), while other regions are nonlinearly stabilized. The unstable band is broader at $k_x>0$, as indicated in Fig. 6 which shows the energy input rate as a function of k_x and k_y. The maximum value of γ^{nl} exceeds the maximum linear growth rate by a factor of 4–5. Thus, the nonlinear instability has a significant effect on growth rates, markedly increasing the driving of certain modes. However, the wave number region of unstable modes is also significantly reduced. Modes both at low k_y and just above $k_y=8$ are unstable at infinitesimal amplitude, extracting free energy from the gradients, but at finite amplitude become energy sinks. This finite amplitude-induced stabilization of linearly unstable low k modes represents a notable change in the growth rate spectrum shape. The modes along the $k_y=0$ axis constitute a zonally averaged flow, i.e., $\langle \nu_y \rangle_y \equiv \int dy\ \nu_y = \int dk_x \exp(ik_x x) ik_x \phi_{k_x,k_y}=0$. These modes are in the dissipative regime for all values of $\upsilon \neq 0$ because $k_y \nu_D = 0$. At infinitesimal amplitude they are marginally

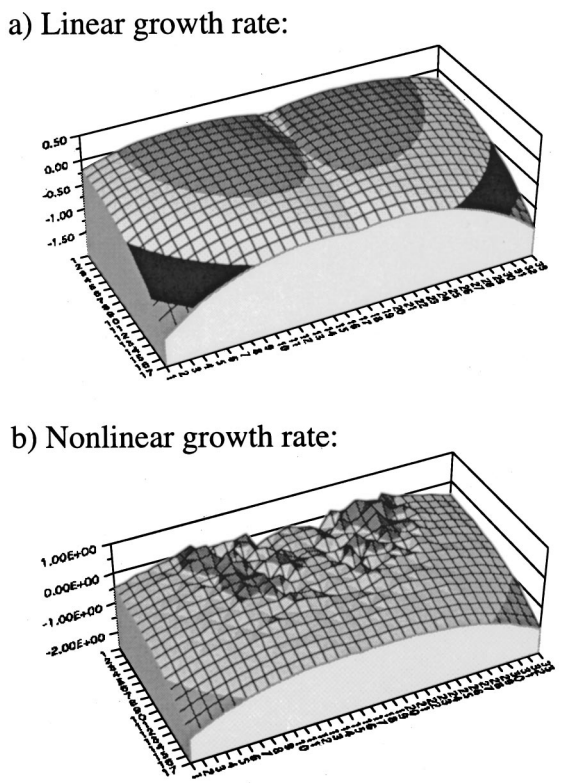

FIG. 6. Energy input rate as a function of k_x and k_y in (a) linear growth phase, and (b) saturated state.

stable ($\mathrm{Im}\,\omega=0$), and are seen as a crease in Fig. 6(a). At finite amplitude these modes are damped. The damping rate is a non-negligible fraction of the maximum growth rate. The damping of zonal flows has an important effect on the turbulence level in simulations of gyrokinetic models.[20] Note that here the finite excitation level for these undriven modes, as indicated by the spectrum, indicates spectral transfer into these modes via nonlinear coupling. This is the standard excitation mechanism for zonal modes.[21] The finite amplitude-induced damping evident in Fig. 6 is a distinct process arising from damped eigenmode excitation, and is currently being investigated.[22]

In Fig. 7 the quasilinear particle flux for different values of $\hat{\alpha}$ is plotted as a function of the true flux. The two are clearly different, with the true flux smaller than the quasilinear flux by a factor of order 5. The flux is essentially a wave number moment of $\gamma^{nl}(k)\,E(k)$. The reduction of the true flux relative to the quasilinear flux reflects the fact that $\gamma^{nl}(k)$ is smaller than $\gamma^{l}(k)$ for low wave numbers where $E(k)$ peaks. Wave numbers where $\gamma^{nl}(k)$ is greater than $\gamma^{l}(k)$ receive weaker weighting in the wave number sum, because $E(k)$ is smaller. In simulations of nonadiabatic Hasegawa–Wakatani turbulence, a reduction of the particle flux from its quasilinear value was observed and attributed to spatial intermittency, i.e., coherent structures.[23] The nonlinear instability mechanism described herein is not caused by intermittency, because coherent structures are not accounted for in the analytic theory (which is quasi-Gaussian) and are not present in the simulations. The latter is confirmed in Fig. 8, which shows contours of constant density in real space.

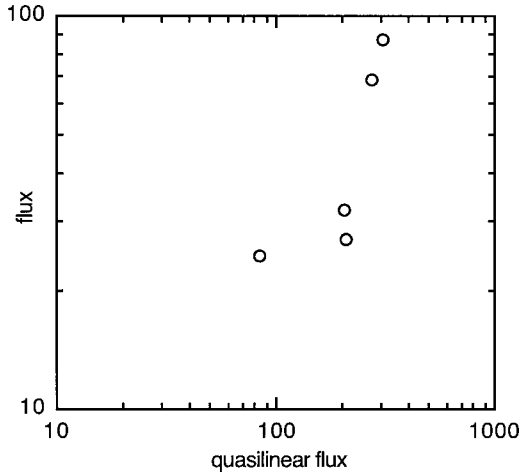

FIG. 7. Quasilinear flux versus actual flux for values of $\hat{\alpha}$ varied over a range of 2.

The packing fraction (roughly, the ratio of structure scale to interstructure separation) is approximately unity, an indication that the kurtosis is near 3 and the distribution is close to Gaussian. While intermittency may be possible in Eqs. (1)–(2) under appropriate circumstances, we conclude that it is not a necessary element of the particle flux reduction described above. The question of intermittency in this system is interesting, but beyond the scope of this paper.

IV. NONLINEAR EXCITATION OF THE DAMPED EIGENMODE

Because nonlinear instability requires nonlinear excitation of the purely stable eigenmode branch, it is advanta-

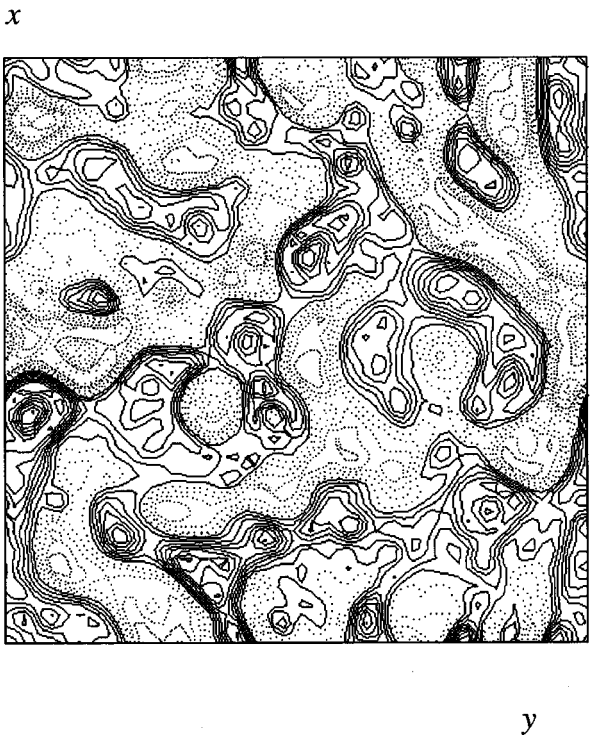

FIG. 8. Contours of constant density during saturation. The packing fraction of structures is near unity, indicating that the kurtosis is close to the Gaussian value of 3.

geous to transform the basic equations so they describe the nonlinear evolution of the two linear eigenmode branches, i.e., use Eq. (11) to project at each moment in time the density and potential onto the two linear eigenmodes of Eqs. (5) and (7). To develop equations for the nonlinearly evolving eigenmode amplitudes β_j we rewrite Eqs. (1)–(2) in matrix form

$$\begin{pmatrix} \dot{n}_k \\ \dot{\phi}_k \end{pmatrix} = \mathbf{D} \begin{pmatrix} n_k \\ \phi_k \end{pmatrix} + \begin{pmatrix} b_n \\ b_\phi \end{pmatrix}, \tag{14}$$

where $\mathbf{D}$ is the linear coupling matrix and b_n and b_ϕ are the nonlinearities

$$\mathbf{D} = \begin{pmatrix} -\upsilon & -ik_y \nu_D \hat{\alpha} + \upsilon \\ \dfrac{\varepsilon^{1/2}\upsilon}{1+k^2-\varepsilon^{1/2}} & \dfrac{-k_y \nu_D \hat{\alpha} - \varepsilon^{1/2}\upsilon}{1+k^2-\varepsilon^{1/2}} \end{pmatrix}, \tag{15}$$

$$b_n = -\frac{1}{2}\sum_{k'} (\mathbf{k}' \times \mathbf{z} \cdot \mathbf{k})(n_{k'}\phi_{k-k'} - n_{k-k'}\phi_{k'}), \tag{16}$$

$$b_\phi = -\frac{1}{2}\sum_{k'} \frac{(\mathbf{k}' \times \mathbf{z} \cdot \mathbf{k})}{1+k^2-\varepsilon^{1/2}} [(k-k')^2 - k'^2]\phi_{k'}\phi_{k-k'}. \tag{17}$$

We invert Eq. (11), take the time derivative, and substitute from Eq. (14), yielding

$$\begin{pmatrix} \dot{\beta}_1(k,t) \\ \dot{\beta}_2(k,t) \end{pmatrix} = \mathbf{M}^{-1} \begin{pmatrix} \dot{n}_k \\ \dot{\phi}_k \end{pmatrix} = \mathbf{M}^{-1}\mathbf{D} \begin{pmatrix} n_k \\ \phi_k \end{pmatrix} + \mathbf{M}^{-1} \begin{pmatrix} b_n \\ b_\phi \end{pmatrix}, \tag{18}$$

where

$$\mathbf{M}^{-1} = \frac{1}{R_1 - R_2} \begin{pmatrix} 1 & -R_2 \\ -1 & R_1 \end{pmatrix}. \tag{19}$$

To complete the transformation, n_k and ϕ_k must be written in terms of β_1 and β_2 using Eq. (11)

$$\begin{pmatrix} \dot{\beta}_1(k,t) \\ \dot{\beta}_2(k,t) \end{pmatrix} = \mathbf{M}^{-1}\mathbf{D}\mathbf{M} \begin{pmatrix} \beta_1(k,t) \\ \beta_2(k,t) \end{pmatrix} + \mathbf{M}^{-1} \begin{pmatrix} b_n \\ b_\phi \end{pmatrix}\Bigg|_{\substack{n_k = R_1\beta_1 + R_2\beta_2 \\ \phi_k = \beta_1 + \beta_2}}. \tag{20}$$

By construction, this representation diagonalizes the linear coupling matrix, i.e., $\mathbf{M}^{-1}\mathbf{D}\mathbf{M}$ is diagonal with the eigenfrequencies $-i\omega_1$ and $-i\omega_2$ as the diagonal elements. However, in this representation each equation evolves under a combination of the two nonlinearities. From $\mathbf{M}^{-1}$, the nonlinearity of the β_1 equation is $(R_1-R_2)^{-1}(b_n - R_2 b_\phi)$, while the nonlinearity of the β_2 equation is $(R_1-R_2)^{-1}(-b_n + R_1 b_\phi)$. Noting that $R_2 \sim (k_y \nu_D/\upsilon)R_1$, this validates the statement made in Sec. II that the electron nonlinearity yields forces in the β_1 and β_2 equations of equal magnitude, while the polarization drift nonlinearity preferentially forces the growing eigenmode. As indicated in Eq. (20), the nonlinearities are written in terms of β_1 and β_2 using the substitutions $n_k = R_1\beta_1 + R_2\beta_2$ and $\phi_k = \beta_1 + \beta_2$ in Eqs. (16)–(17).

To simplify Eq. (20), we examine the relative magnitude of the nonlinearities. To compare b_n and b_ϕ, first assume that $n_k \sim \phi_k$, as in the unstable eigenmode. The electron nonlinearity b_n has two fewer factors of wave number than the polarization drift nonlinearity b_ϕ. Hence, in a long-wavelength regime $(k<1) b_n$ dominates b_ϕ. Consider now a density fluctuation like the stable eigenmode. The electron nonlinearity continues to dominate at long wavelengths because it still has fewer factors of wave number (one in this case), but n is now larger than ϕ by a factor of order $k_y \nu_D/\upsilon \gg 1$. Consequently, the electron nonlinearity dominates at long wavelengths for collisionless trapped electron turbulence. The degree of dominance is greater than it is in the collisional case, where the electron nonlinearity has one fewer wave number factor than the polarization drift nonlinearity, and $n_k \sim \phi_k$. The dominance of the electron nonlinearity in the collisional regime has been studied in detail.[24] We will restrict ourselves to long wavelengths. Simplifying Eq. (20) by retaining the electron nonlinearity only

$$\dot{\beta}_j(k) = -i\omega_j\beta_j(k) + \sum_{k'} \frac{(-1)^j(\mathbf{k}' \times \mathbf{z} \cdot k)}{[R_1(k) - R_2(k)]} \times [R_1(k')\beta_1(k') + R_2(k')\beta_2(k')][\beta_1(k'') + \beta_2(k'')], \tag{21}$$

where $R_1(k)$ and $R_2(k)$ are defined in Eqs. (5) and (7), and $k'' \equiv k - k'$. It is possible to make one additional approximation. Because β_1 is linearly driven and β_2 is linearly damped, the former is larger than the latter in saturation. This is evident in the simulations described in the previous section. From the saturation balance obtained in Sec. V, $\mathrm{Im}\,\beta_2 \sim (\upsilon/\nu_D k_y)|\beta_1|$, and $\mathrm{Re}\,\beta_2 \sim (\upsilon/\nu_D k_y)^2|\beta_1|$. This allows $\beta_2(k'')$ in the last set of brackets to be dropped. The term with $\beta_2(k')$ in the first set of brackets cannot be dropped because $R_2/R_1 \sim \mathrm{O}(i\nu_D k_y/\upsilon)$, making $R_2(k')\beta_2(k')$ as large as $R_1(k')\beta_1(k')$. It can be verified that the terms omitted by dropping $\beta_2(k'')$ conserve energy among themselves. Therefore, Eq. (21), with $\beta_2(k'')$ removed, is an energy-conserving approximation. Consequently, we shall henceforth investigate the nonlinear evolution of

$$\dot{\beta}_j(k) = -i\omega_j\beta_j(k) + \sum_{k'} \frac{(-1)^j(\mathbf{k}' \times \mathbf{z} \cdot k)}{[R_1(k) - R_2(k)]} \times [R_1(k')\beta_1(k') + R_2(k')\beta_2(k')]\beta_1(k''). \tag{22}$$

We first examine the nonlinear excitation of $\beta_2(k)$. From an initial state with infinitesimal amplitudes, the nonlinearities are at first negligible, and β_1 and β_2 evolve according to the linearized equations. The exponential growth of β_1 and the exponential decay of β_2 produce a situation where in one or two linear growth times, $\beta_2 \ll \beta_1$, and the nonlinearity is dominated by β_1. Assuming $\beta_2 \ll \beta_1$ and symmetrizing the remaining nonlinearity, Eq. (22) becomes

$$\dot{\beta}_2(k)+i\omega_2\beta_2(k)\cong\sum_{k'}\frac{(\mathbf{k}'\times\mathbf{z}\cdot k)}{2[R_1(k)-R_2(k)]}[R_1(k')-R_1(k-k')]\beta_1(k')\beta_1(k'')$$

$$\cong\sum_{k'}(\mathbf{k}'\times\mathbf{z}\cdot k)\beta_1(k')\beta_1(k-k')\left\{\frac{i\upsilon\varepsilon^{1/2}\hat{\alpha}\mathbf{k}\cdot\mathbf{k}'}{(1-\hat{\alpha}\varepsilon^{1/2})^2k_y\nu_D}-\frac{\upsilon^2\varepsilon^{1/2}(1-\varepsilon^{1/2})(\hat{\alpha}-1)}{2(1-\hat{\alpha}\varepsilon^{1/2})^4\nu_D^2k_y^2}\left(\frac{k_y}{k_y'}-\frac{k_y}{k_y-k_y'}\right)\right\},\qquad(23)$$

where $k\ll 1$ has been assumed. The first term of the last expression is of order $\upsilon/k_y\nu_D$, and small-k contributions of order kk' have been retained. These contributions have been neglected in the second term, which is one order higher in $\upsilon/k_y\nu_D$. From these expressions it is evident that β_1 and β_2 evolve linearly until β_1 exceeds an amplitude threshold governed by the magnitude of the nonlinearity relative to $\omega_j\beta_j$. The threshold is lower for the β_2 evolution because β_2 decreases with time in the linear regime, whereas β_1 increases. The nonlinear threshold in the β_2 equation is given by

$$\frac{\upsilon}{\nu_D}[\beta_1^{(l)}]^2\approx|\omega_2\beta_2^{(l)}|,\qquad(24)$$

where $\beta_j^{(l)}\equiv\exp(-i\omega_jt)\beta_j(k,t=0)$ represents the linear solution of Eq. (22), which is valid up to the time the nonlinear threshold is reached. Because $\beta_1^{(l)}$ must reach a higher amplitude before the β_1 equation becomes nonlinear, the nonlinear evolution of β_2 (upon passing its nonlinear threshold) can be approximated using the linearized solution $\beta_1^{(l)}$. Thus,

$$\beta_2(k,t)=\beta_2(k,t=0)\exp[-i\omega_2(k)t]+\sum_{k'}(\mathbf{k}'\times\mathbf{z}\cdot\mathbf{k})$$
$$\times\left\{\frac{i\upsilon\varepsilon^{1/2}\hat{\alpha}\mathbf{k}\cdot\mathbf{k}'}{(1-\hat{\alpha}\varepsilon^{1/2})^2k_y\nu_D}-\frac{\upsilon^2\varepsilon^{1/2}(1-\varepsilon^{1/2})(\hat{\alpha}-1)}{2(1-\hat{\alpha}\varepsilon^{1/2})^4\nu_D^2k_y^2}\right.$$
$$\left.\times\left(\frac{k_y}{k_y'}-\frac{k_y}{k_y-k_y'}\right)\right\}\beta_1(k',t=0)$$
$$\times\beta_1(k-k',t=0)$$
$$\times\frac{\{\exp[-i\omega_1(k')t-i\omega_1(k-k')t]\}}{i[\omega_2(k)-\omega_1(k')-\omega_1(k-k')]}.\qquad(25)$$

From Eq. (25) both linear decay (first term) and nonlinearly driven exponential growth (second term) operate simultaneously, but decay dominates prior to the transition, and growth thereafter. The growth rate is controlled by the largest value of $-i\omega_1(k')-i\omega_1(k-k')$ in the sum over k'. In Fig. 2 exponential growth occurs for $20<t<50$. Similarly, Eq. (25) indicates that before the transition the frequency of β_2 is nearly zero, whereas after it is of order ν_Dk_y. Therefore, the frequency spectrum peak shifts in the transition from near zero to $\sim\nu_Dk_y$, as evident in Fig. 3.

The exponential growth of β_1 saturates when

$$\frac{\upsilon}{\nu_D}[\beta_1^{(l)}]^2\approx\mathrm{Im}\,\omega_1|\beta_{1,}^{(l)}|.\qquad(26)$$

Unlike the nonlinear excitation of β_2, which is phase coherent as long as β_1 is growing linearly (and therefore phase coherent), the nonlinear evolution (saturation) of $\beta_1(k,t)$ involves mode coupling and phase scrambling. A description of saturation thus requires a statistical treatment.

V. CLOSURE CALCULATION

Equation (26) is valid as long as β_1 grows exponentially, experiencing negligible feedback from β_2. This situation no longer holds as the instability saturates. To describe saturation we introduce closure theory. A variety of insights is obtained from closure theory. It reveals a direct relationship between nonlinear instability and the nonlinear excitation of modes on the purely stable branch by showing that the requirement for energy transfer to these modes favors nonlinear instability. It also shows that the system has volatility with respect to the sign of γ_k^{nl}, i.e., both signs are possible and likely, as observed in the simulations. Moreover, whereas other studies of two-field drift wave models have emphasized the role of the density-potential cross correlation in inhibiting the turbulent energy cascade[25] the closure calculation shows that the cross-correlation value fixed by the nonlinear dynamics in saturation *enhances* the nonlinear energy transfer to the stable branch. Since the latter provides coupling to dissipation within a single nonlinear interaction, less cascading is required for saturation.

The closure equations are complicated and possess many terms. The solution given herein consists of the following. In Sec. V A, leading order asymptotic scalings are found for the quantities, $|\beta_1|^2$, $|\beta_2|^2$, $\mathrm{Re}\langle\beta_1^*\beta_2\rangle$, and $\mathrm{Im}\langle\beta_1^*\beta_2\rangle$, as a function of υ/ν_Dk_y, the small parameter of the low collisionality limit. Because the growth rate $\mathrm{Im}\,\omega_1$ and the damping rate $\mathrm{Im}\,\omega_2$ enter the lowest-order balances for $|\beta_1|^2$ and $|\beta_2|^2$, respectively, these scalings recover the saturation level of each quantity to leading order in the low collisionality limit, up to a numerical coefficient of order unity. The coefficients of $|\beta_1|^2$ and $|\beta_2|^2$ are positive; those of $\mathrm{Re}\langle\beta_1^*\beta_2\rangle$, and $\mathrm{Im}\langle\beta_1^*\beta_2\rangle$ can be either positive or negative. The signs are determined from the equations for $|\beta_2|^2$ and $\mathrm{Re}\langle\beta_1^*\beta_2\rangle$. With this solution we examine the energy input rate in Sec. V B.

A. Saturation balances

Statistical closure equations for $|\beta_1|^2$, $|\beta_2|^2$, and $\langle\beta_1^*\beta_2\rangle$ are constructed from Eq. (22) by multiplying by appropriate amplitude factors. Calculating a closure for all linear eigenmode branches differs from the usual procedure, which treats Fourier transformed equations for n and ϕ [Eq. (14)], with ω replaced by ω_1. The latter, by construction, describes saturation as the Kolmogorov-style steady state in which unstable modes saturate through transfer of energy to stable modes within the same branch.[12–14,25] On the other hand, solution of spectrum balance equations for all linear eigenmodes completely specifies the nonlinear eigenmode.

Taking moments of Eq. (22), the evolution equations for the quadratic correlations $|\beta_1|^2$, $|\beta_2|^2$, and $\langle\beta_1^*\beta_2\rangle$ are

$$\frac{\partial}{\partial t}|\beta_1|^2 = 2\,\mathrm{Im}\,\omega_1|\beta_1|^2 + 2\,\mathrm{Re}\sum_{k'}\left[\frac{C_1(k,k')}{2}\langle\beta_1'\beta_1''\beta_1^*\rangle + C_2(k,k')\langle\beta_2'\beta_1''\beta_1^*\rangle\right], \tag{27}$$

$$\frac{\partial}{\partial t}|\beta_2|^2 = 2\,\mathrm{Im}\,\omega_2|\beta_2|^2 - 2\,\mathrm{Re}\sum_{k'}\left[\frac{C_1(k,k')}{2}\langle\beta_1'\beta_1''\beta_1^*\rangle + C_2(k,k')\langle\beta_2'\beta_1''\beta_2^*\rangle\right], \tag{28}$$

$$\frac{\partial}{\partial t}\langle\beta_1^*\beta_2\rangle = i(\omega_1^* - \omega_2)\langle\beta_1^*\beta_2\rangle + \sum_{k'}\left[\frac{C_1^*(k,k')}{2}\langle\beta_1'^*\beta_1''^*\beta_2\rangle - C_2^*(k,k')\langle\beta_2'^*\beta_1''^*\beta_2\rangle - \frac{C_1(k,k')}{2}\langle\beta_1'\beta_1''\beta_1^*\rangle + C_2(k,k')\langle\beta_2'\beta_1''\beta_1^*\rangle\right], \tag{29}$$

where

$$C_1(k,k') = -(\mathbf{k}'\times\mathbf{z}\cdot\mathbf{k})\frac{(R_1'-R_1'')}{(R_1-R_2)}, \tag{30}$$

$$C_2(k,k') = -(\mathbf{k}'\times\mathbf{z}\cdot\mathbf{k})\frac{R_2}{(R_1-R_2')}, \tag{31}$$

and the notation $\beta_j' = \beta_j(k')$, $\beta_j'' = \beta_j(k-k')$, $\beta_j = \beta_j(k)$, $R_j' = R_j(k')$, $R_j'' = R_j(k-k')$, and $R_j = R_j(k)$ has been used for shorthand.

Equations (27)–(29) are not closed because they depend on the unknown triplet correlations of the right-hand side. To close we use the EDQNM procedure. The procedure is standard and given in other references; hence, we omit intermediate steps. We start by finding evolution equations for each triplet in Eqs. (27)–(29), multiplying Eq. (22) (for appropriate wave numbers) by appropriate products of $\beta_1\beta_2$ and $\beta_1\beta_2$. These equations contain fourth-order correlations, which are approximated as products of second-order correlations. Treating the products of second-order correlations as slowly evolving source terms, the triplet evolution equations are inverted and substituted into Eqs. (27)–(29), yielding a set of equations closed at second order. The third-order correlations are subject to eddy damping, which is specified self-consistently in the closure. The closed second-order equations are

$$\begin{aligned}\frac{\partial}{\partial t}|\beta_1|^2 = {} & 2\,\mathrm{Im}\,\omega_1|\beta_1|^2 + \mathrm{Re}\sum_{k'}\left\{\frac{1}{2}\frac{C_1(k,k')}{(i\omega_1' + i\omega_1'' - i\omega_1^* - \Delta\omega_1' - \Delta\omega_1'' - \Delta\omega_1^*)}\right. \\ & [C_1(k',k)|\beta_1''|^2|\beta_1|^2 \\ & + C_1(k-k',k)|\beta_1'|^2|\beta_1|^2 + C_1^*(k,k')|\beta_1'|^2|\beta_1''|^2 + C_2(k',-k'')|\beta_1|^2\langle\beta_1''\beta_2''^*\rangle \\ & + C_2(k',k)|\beta_1''|^2\langle\beta_1^*\beta_2\rangle + C_2(k'',k)|\beta_1'|^2\langle\beta_1^*\beta_2\rangle + C_2(k'',-k')|\beta_1|^2\langle\beta_1'\beta_2'^*\rangle + C_2^*(k,k')|\beta_1''|^2\langle\beta_1'\beta_2'^*\rangle \\ & + C_2^*(k,k'')|\beta_1'|^2\langle\beta_1''\beta_2''^*\rangle] + \frac{C_2(k,k')}{(i\omega_2' + i\omega_1'' - i\omega_1^* - \Delta\omega_2' - \Delta\omega_1'' - \Delta\omega_1^*)}[C_1(k'',k)|\beta_1|^2\langle\beta_1'^*\beta_2'\rangle \\ & - C_1(k',k)|\beta_1''|^2|\beta_1|^2 + C_1^*(k,k')|\beta_1''|^2\langle\beta_1'^*\beta_2'\rangle + C_2(k'',k)\langle\beta_1'^*\beta_2'\rangle\langle\beta_1^*\beta_2\rangle \\ & + C_2(k'',-k')|\beta_1|^2|\beta_2'|^2 - C_2(k',k)|\beta_1''|^2\langle\beta_1^*\beta_2\rangle - C_2(k',-k'')\langle\beta_1''\beta_2''^*\rangle|\beta_1|^2 \\ & \left. + C_2^*(k,k')|\beta_1''|^2|\beta_2'|^2 + C_2^*(k,k'')\langle\beta_1''\beta_2''^*\rangle\langle\beta_1'^*\beta_2'\rangle]\right\},\end{aligned} \tag{32}$$

$$\begin{aligned}\frac{\partial}{\partial t}|\beta_2|^2 = {} & 2\,\mathrm{Im}\,\omega_2|\beta_2|^2 - \mathrm{Re}\sum_{k'}\left\{\frac{1}{2}\frac{C_1(k,k')}{(i\omega_1' + i\omega_1'' - i\omega_2^* - \Delta\omega_1' - \Delta\omega_1'' - \Delta\omega_2^*)}\right. \\ & \times[C_1(k',k)|\beta_1''|^2\langle\beta_1\beta_2^*\rangle + C_1(k-k',k)|\beta_1'|^2\langle\beta_1\beta_2^*\rangle - C_1^*(k,k')|\beta_1'|^2|\beta_1''|^2 + C_2(k',-k'')\langle\beta_1\beta_2^*\rangle\langle\beta_1''\beta_2''^*\rangle \\ & + C_2(k',k)|\beta_1''|^2|\beta_2|^2 + C_2(k'',k)|\beta_1'|^2|\beta_2|^2 + C_2(k'',-k')\langle\beta_1\beta_2^*\rangle\langle\beta_1'\beta_2'^*\rangle - C_2^*(k,k')|\beta_1''|^2\langle\beta_1'\beta_2'^*\rangle \\ & - C_2^*(k,k'')|\beta_1'|^2\langle\beta_1''\beta_2''^*\rangle] + \frac{C_2(k,k')}{(i\omega_2' + i\omega_1'' - i\omega_2^* - \Delta\omega_2' - \Delta\omega_1'' - \Delta\omega_2^*)}[C_1(k'',k)\langle\beta_1\beta_2^*\rangle\langle\beta_1'^*\beta_2'\rangle \\ & - C_1(k',k)\langle\beta_1\beta_2^*\rangle|\beta_1''|^2 - C_1^*(k,k')|\beta_1''|^2\langle\beta_1'^*\beta_2'\rangle + C_2(k'',k)\langle\beta_1'^*\beta_2'\rangle|\beta_2|^2 + C_2(k'',-k')\langle\beta_1\beta_2^*\rangle|\beta_2'|^2 \\ & \left. - C_2(k',k)|\beta_2|^2|\beta_1''|^2 - C_2(k',-k'')\langle\beta_1\beta_2^*\rangle\langle\beta_2''^*\beta_1''\rangle - C_2^*(k,k')|\beta_1''|^2|\beta_2'|^2 - C_2^*(k,k'')\langle\beta_1''\beta_2''^*\rangle\langle\beta_1'^*\beta_2'\rangle]\right\},\end{aligned} \tag{33}$$

$$\frac{\partial}{\partial t}\langle\beta_1^*\beta_2\rangle = i(\omega_1^*-\omega_2)\langle\beta_1^*\beta_2\rangle + \sum_{k'}\left\{\frac{1}{2}\frac{C_1^*(k,k')}{(-i\omega_1'^*-i\omega_1''^*+i\omega_2-\Delta\omega_1'^*-\Delta\omega_1''^*-\Delta\omega_2)}\right.$$
$$\times[2C_1^*(k'',k)|\beta_1'|^2\langle\beta_1^*\beta_2\rangle+2C_2^*(k'',k)|\beta_1'|^2|\beta_2|^2+2C_2^*(k'',-k')\langle\beta_1'^*\beta_2'\rangle\langle\beta_1^*\beta_2\rangle-C_1(k,k')|\beta_1'|^2|\beta_1''|^2$$
$$-2C_2^*(k,k'')|\beta_1'|^2\langle\beta_1''\beta_2''^*\rangle]-\frac{C_2^*(k,k')}{(-i\omega_1''^*-i\omega_2'^*+i\omega_2-\Delta\omega_1''^*-\Delta\omega_2'^*-\Delta\omega_2)}$$
$$\times[C_1^*(k'',k)\langle\beta_1^*\beta_2\rangle\langle\beta_1'\beta_2'^*\rangle-C_1^*(k',k)\langle\beta_1^*\beta_2\rangle|\beta_1''|^2-C_1^*(k,k')\langle\beta_1'\beta_2'^*\rangle|\beta_1''|^2$$
$$+C_2^*(k'',k)|\beta_2|^2\langle\beta_1'\beta_2'^*\rangle+C_2^*(k'',k)|\beta_2'|^2\langle\beta_1^*\beta_2\rangle-C_2^*(k',k)|\beta_2|^2|\beta_1''|^2-C_2^*(k',-k'')\langle\beta_1^*\beta_2\rangle\langle\beta_2''\beta_1''^*\rangle$$
$$-C_2(k,k')|\beta_1'|^2|\beta_1''|^2-C_2(k,k'')\langle\beta_1'\beta_2'^*\rangle\langle\beta_1''^*\beta_2''\rangle]-\frac{1}{2}\frac{C_1(k,k')}{(i\omega_1'+i\omega_1''-i\omega_1^*-\Delta\omega_1'-\Delta\omega_1''-\Delta\omega_1^*)}$$
$$\times[2C_1(k'',k)|\beta_1'|^2|\beta_1|^2+2C_2(k'',k)|\beta_1'|^2\langle\beta_1^*\beta_2\rangle+2C_2(k'',-k')|\beta_1|^2\langle\beta_1'\beta_2'^*\rangle-C_1^*(k,k')|\beta_1'|^2|\beta_1''|^2$$
$$+2C_2^*(k,k'')|\beta_1'|^2\langle\beta_1''\beta_2''^*\rangle]+\frac{C_2(k,k')}{(i\omega_1''+i\omega_2'-i\omega_1^*-\Delta\omega_1''-\Delta\omega_2'-\Delta\omega_2^*)}$$
$$\times[C_1(k'',k)|\beta_1|^2\langle\beta_1'^*\beta_2'\rangle-C_1(k',k)|\beta_1|^2|\beta_1''|^2+C_1^*(k,k')\langle\beta_1'^*\beta_2'\rangle|\beta_1''|^2+C_2(k'',k)\langle\beta_1^*\beta_2\rangle\langle\beta_1'^*\beta_2'\rangle$$
$$-C_2(k',k)|\beta_1''|^2\langle\beta_1^*\beta_2\rangle+C_2(k'',-k')|\beta_2'|^2|\beta_1|^2-C_2(k',-k'')\langle\beta_1''\beta_2''^*\rangle|\beta_1|^2+C_2^*(k,k')|\beta_2'|^2|\beta_1''|^2$$
$$\left.+C_2(k,k'')\langle\beta_1'^*\beta_2'\rangle\langle\beta_1''\beta_2''^*\rangle]\right\}. \tag{34}$$

The frequencies $\Delta\omega_1$ and $\Delta\omega_2$ are the eddy damping rates, obtained as the eigenfrequencies of the finite-amplitude response of β_1 and β_2 to an infinitesimal impulse. These rates are given by

$$\Delta\omega_1=\sum_{k'}\left\{\frac{1}{2}\frac{C_1(k,k')}{(i\omega_1'+i\omega_1''-\Delta\omega_1'-\Delta\omega_1'')}[C_1(k'',k)|\beta_1'|^2+C_1(k',k)|\beta_1''|^2+C_2(k',-k'')\langle\beta_1''\beta_2''^*\rangle+C_2(k'',-k')\langle\beta_1'\beta_2'^*\rangle]\right.$$
$$-\frac{C_2(k,k')}{(i\omega_2'+i\omega_1''-\Delta\omega_2'-\Delta\omega_1'')}\times[C_1(k'',k)\langle\beta_1'^*\beta_2'\rangle+C_2(k'',-k')|\beta_2'|^2+C_1(k',k)|\beta_1''|^2$$
$$\left.+C_2(k',-k'')\langle\beta_1''\beta_2''^*\rangle]\right\}, \tag{35}$$

$$\Delta\omega_2=-\sum_{k'}\left\{\frac{1}{2}\frac{C_1(k,k')}{(i\omega_1'+i\omega_1''-\Delta\omega_1'-\Delta\omega_1'')}[C_2(k'',k)|\beta_1'|^2+C_2(k',k)|\beta_1''|^2]-\frac{C_2(k,k')}{(i\omega_2'+i\omega_1''-\Delta\omega_2'-\Delta\omega_1'')}\right.$$
$$\left.\times[C_2(k'',k)\langle\beta_1'^*\beta_2'\rangle+C_2(k',k)|\beta_1''|^2]\right\}. \tag{36}$$

Solution of Eqs. (32)–(36) specifies $|\beta_1(k)|^2$, $|\beta_2(k)|^2$, $\langle\beta_1^*(k)\beta_2(k)\rangle$, $\Delta\omega_1(k)$, and $\Delta\omega_2(k)$, as functions of both wave number and the parameters ν, ω_*, $\varepsilon^{1/2}$, and $\hat{\alpha}$ of the linear instability drive and nonlinear couplings. Even for the simpler saturation balances of one-field closures, the nonlinear spectrum convolutions make evaluation of the spectrum intractable in any range of wave numbers for which there is instability or dissipation. A simpler task is to determine the saturation levels of $|\beta_1|^2$, $|\beta_2|^2$, and $\langle\beta_1^*\beta_2\rangle$ for low wave number unstable modes due to nonlinear coupling with modes at higher wave number. The saturation levels are expressed as functions of the parameters ν, ω_*, $\varepsilon^{1/2}$, and $\hat{\alpha}$ that enter the linear growth rate and the nonlinear couplings.

We seek leading order asymptotic scalings for the saturated values of $|\beta_1|^2$, $|\beta_2|^2$, and $\langle\beta_1^*\beta_2\rangle$ as functions of $\nu/\omega_*\ll 1$. This is done by testing trial scalings to see if the dominant balances in Eqs. (32)–(36) meet the two fundamental physical constraints of the saturated state. The constraints are: (1) The dominant balance in the $|\beta_1|^2$ equation must contain the linear driving term 2 Im $\omega_1|\beta_1|^2$. This is the source of free energy for exciting turbulence and must be present in the dominant balance. (2) The dominant balance in the $|\beta_2|^2$ equation must contain the linear damping term 2 Im $\omega_2|\beta_2|^2$. The excitation of β_2 described in Sec. IV effectively establishes a cascade *in eigenmode space* at fixed wave number. With $|\beta_2|^2$ subject to strong linear damping, it is in a dissipation range, and the damping enters the balance. Implicit in this condition is the inequality $|\beta_1|^2\gg|\beta_2|^2$, which as noted in Sec. III is satisfied by the numerical solutions. In addition to these constraints, we assume that inco-

herent terms are small and exclude them from saturation balances *a priori*. This assumption applies to spectral transfer from a mode k to short wavelength modes k', $k-k' \gg k$. Provided the spectrum decays with wave number, the product $|\beta_j'|^2|\beta_i''|^2$ of an incoherent term is smaller than its coherent counterpart $|\beta_j|^2|\beta_i'|^2$ because the former is quadratic in high wave number energy, whereas the latter is linear. Moreover, incoherent terms are identified with the production of turbulence in an inertial range. However, in driven ranges production is by linear instability, and the incoherent terms are small.

To establish the scaling of each term in Eqs. (32)–(36), we must know the scaling of the temporal response functions. The temporal response functions appear in Eqs. (32)–(36) as denominators comprised of combinations of $i\omega_1$, $i\omega_2$, $\Delta\omega_1$, and $\Delta\omega_2$. Consider the first response function of Eq. (33): $(i\omega_1'+i\omega_1''-i\omega_2^*-\Delta\omega_1'-\Delta\omega_1''-\Delta\omega_2^*)^{-1}$. The first three terms are linear eigenfrequencies and together go as $\sim i\nu_D[k_y'-(k_y-k_y')][1-\varepsilon^{1/2}\hat{\alpha}]=-\nu_D k_y[1-\varepsilon^{1/2}\hat{\alpha}]$ to lowest order in v/ω_*' for k^2 and $\varepsilon^{1/2}$ small. The real parts of the eddy damping rates are of order v because of the balances in conditions (1) and (2) above. As shown below, $\mathrm{Im}\,\Delta\omega_1 \sim v^2/\omega_*$, $\mathrm{Im}\,\omega_2 \sim \omega_*$. Thus, the entire response function scales as $(-iak_y\nu_D+bv)^{-1}$, where a and b are constants of order unity. It is easily verified that all of the response functions of Eqs. (32)–(34) have this scaling except for one. The exception is the response function $(i\omega_1'+i\omega_1''-i\omega_1^*-\Delta\omega_1'-\Delta\omega_1''-\Delta\omega_1^*)^{-1}$ appearing in Eqs. (32) and (34). Under the nearly dispersionless character of ω_1 at low k, the leading order contributions of each of the first three terms cancel provided $\nu_D k_y k^2 \ll v$. This propagator therefore scales as $(a'v+ib'v^2/k_y\nu_D)$, where a' and b' are constants of order unity. The difference between this propagator and the others is crucial in setting transfer rates.

To obtain a set of plausible trial scalings, we start with the condition $|\beta_2|^2 \ll |\beta_1|^2$, and calculate the saturation level of $|\beta_1|^2$ with $|\beta_2|^2 \to 0$. Balancing the first two terms of the nonlinearity in Eq. (31) with the growth rate, we obtain

$$|\beta_1|^2 \approx \nu_D^2\kappa_y^2(\kappa'\times z\cdot\kappa)^{-2}(\kappa\cdot\kappa')^{-2}, \tag{37}$$

where κ and κ' are spectrum weighted wave numbers. This leads us to adopt trial scalings of the form

$$\begin{aligned}
&|\beta_1|^2 \propto (v/\omega_*)^0,\\
&|\beta_2|^2 \propto (v/\omega_*)^{\alpha},\\
&\mathrm{Re}\langle\beta_1^*\beta_2\rangle \propto (v/\omega_*)^{\alpha_r},\\
&\mathrm{Im}\langle\beta_1^*\beta_2\rangle \propto (v/\omega_*)^{\alpha_i}.
\end{aligned} \tag{38}$$

We have specifically examined the cases $(\alpha,\alpha_r,\alpha_i)=(2,1,2)$, $(2,2,1)$, $(1,1/2,3/2)$, $(1,3/2,1/2)$. Of these, all but the second case violate one or both of the physical saturation constraints described above. Remarkably, the second case, $(\alpha,\alpha_r,\alpha_i)=(2,2,1)$, includes every term of Eq. (33) in the dominant balance, and includes all but three terms of Eq. (32). The terms that yield Eq. (37) are included in the dominant balance. Moreover, this case agrees qualitatively with the simulation results. We therefore conclude that the leading order saturation levels are given by

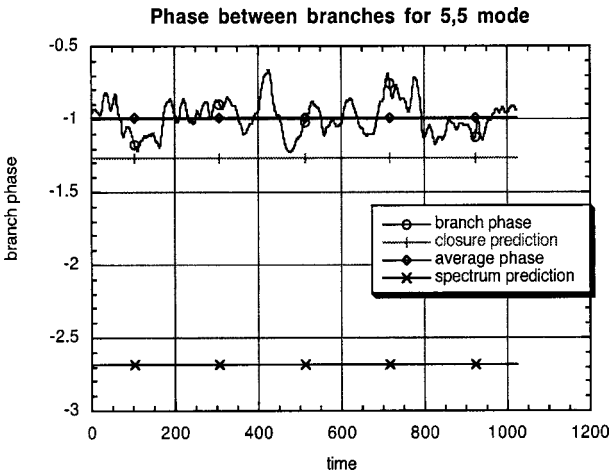

FIG. 9. Time evolution of the complex phase $\tan^{-1}[\mathrm{Im}\langle\beta_1^*\beta_2\rangle/\mathrm{Re}\langle\beta_1^*\beta_2\rangle]$.

$$\begin{aligned}
&|\beta_1|^2 \sim A_1\nu_D^2\kappa_y^2 \quad (v/\nu_D k_y \to 0),\\
&|\beta_2|^2 \sim A_2\nu_D^2\kappa_y^2(v/\nu_D\kappa_y)^2 \quad (v/\nu_D k_y \to 0),\\
&\mathrm{Re}\langle\beta_1^*\beta_2\rangle \sim A_r\nu_D^2\kappa_y^2(v/\nu_D\kappa_y)^2 \quad (v/\nu_D k_y \to 0),\\
&\mathrm{Im}\langle\beta_1^*\beta_2\rangle \sim A_i\nu_D^2\kappa_y^2(v/\nu_D\kappa_y) \quad (v/\nu_D k_y \to 0),
\end{aligned} \tag{39}$$

where A_1, A_2, A_r, and A_i are constants of order unity in the asymptotic expansion, but depend on mean wave numbers in some fashion akin to the wave number dependence of Eq. (37).

The coefficients A_r and A_i can be either positive or negative. As we shall see in Sec. V B, their sign affects the sign of γ^{nl}. We can use the steady-state version of Eq. (33) ($\partial/\partial t \to 0$) to determine the sign of A_i. This is possible because all terms with a factor $\langle\beta_1^*\beta_2\rangle$ or $\langle\beta_1\beta_2^*\rangle$ go as $\mathrm{Im}\langle\beta_1^*\beta_2\rangle$ in leading order. All but one of these terms have coefficients of the same sign, and the sign is such as to require $A_i>0$. With eight terms, A_i is robustly positive. For $A_i>0$, energy is transferred into β_2 from β_1. If A_i were negative energy would be transferred out of β_2, and a steady state could only be possible if $\mathrm{Im}\,\omega_2$ were positive, i.e., if β_2 were linearly unstable. Therefore, $\mathrm{Im}\langle\beta_1^*\beta_2\rangle>0$ controls energy transfer from β_1 to β_2. The eddy damping rates $\Delta\omega_1$ and $\Delta\omega_2$ are also positive if $\mathrm{Im}\langle\beta_1^*\beta_2\rangle>0$. The sign of $\mathrm{Re}\langle\beta_1^*\beta_2\rangle$ must be determined from the imaginary part of Eq. (34) [the real part of Eq. (34) is a function only of $\mathrm{Im}\langle\beta_1^*\beta_2\rangle$ to leading order]. Of the terms proportional to $\mathrm{Re}\langle\beta_1^*\beta_2\rangle$, all but one have coefficients of the same sign. However, the terms not proportional to $\mathrm{Re}\langle\beta_1^*\beta_2\rangle$, which act as a source for $\mathrm{Re}\langle\beta_1^*\beta_2\rangle$, are split almost evenly between positive and negative. The result is $\mathrm{Re}\langle\beta_1^*\beta_2\rangle>0$, but with the nearly even split, $\mathrm{Re}\langle\beta_1^*\beta_2\rangle$ may change signs under different parameter values or spectrum conditions. Thus, $\mathrm{Re}\langle\beta_1^*\beta_2\rangle>0$ is considerably less robust than $\mathrm{Im}\langle\beta_1^*\beta_2\rangle>0$. Figure 9 shows the time evolution of complex phase of $\langle\beta_1^*\beta_2\rangle$ [i.e., $\tan^{-1}(\mathrm{Im}\langle\beta_1^*\beta_2\rangle/\mathrm{Re}\langle\beta_1^*\beta_2\rangle)$] for a wave number corresponding to a nonlinearly unstable mode. The angle is less than $\pi/2$, with $\mathrm{Im}\langle\beta_1^*\beta_2\rangle > \mathrm{Re}\langle\beta_1^*\beta_2\rangle$, and both quantities are positive, in agreement with theory.

The saturation level scalings, Eq. (39), can be substituted into Eqs. (35) and (36) to determine the complex values of the eddy damping rates at saturation. The results are revealing. Equation (35) is dominated by the last two terms, which go as $C_2C_1\beta_1^2$, $C_2^2\langle\beta_1\beta_2\rangle$, yielding $\Delta\omega_1\sim c\nu+id\nu^2/k_y\nu_D$, where c and d are constants of order unity. The real part represents eddy damping at the rate of the linear instability, as required for saturation. The imaginary part is a finite amplitude-induced frequency shift of the unstable eigenmode. This frequency is small compared to the linear frequency ω_1. The last term of Eq. (36) dominates the imaginary part of $\Delta\omega_2$, while this term and several others contribute to the real part in lowest order. The eddy rate is $\Delta\omega_2\sim c'\nu+id'k_y\nu_D$, where c' and d' are constants of order unity. Again, eddy damping is at the rate of the linear instability, consistent with a steady state. The frequency shift, on the other hand, is one order larger than either eddy damping rate or the linear growth rate (which, after all, drives the system), and two orders larger than either $\mathrm{Re}\,\omega_2$ or the frequency shift of the ω_1 branch. This shift, while unusually large, was predicted by the parametric growth analysis of Eq. (25), and evident in Fig. 3. The fact that it is recovered in the closure theory is a check on the validity of the saturation level scalings, and an indication of the predictive power of the closure theory.

The above analysis demonstrates that in saturation there is a nonlinear eigenmode that differs significantly from the eigenmode of the linear instability, for which $A_2=A_r=A_i=0$. The nonlinear eigenmode is reflected in the finite amplitude of the damped eigenmode. Energy transfer to the damped eigenmode, as controlled by $\mathrm{Im}\langle\beta_1^*\beta_2\rangle>0$, provides a saturation mechanism. The terms representing this transfer, and those representing traditional spectral transfer to high wave number within the β_1 fluctuation, are of the same order. Therefore, transfer to the purely stable branch plays a significant role in saturation.

B. Nonlinear growth rate

The energy input rate (nonlinear growth rate) was given in Eq. (10). We write it in terms of β_1 and β_2, substituting Eq. (11) into Eq. (10)

$$2\gamma_k^{nl}E(k)=k_y\nu_D\varepsilon^{1/2}\hat{\alpha}\,\mathrm{Im}\{R_1^*|\beta_1|^2+R_2^*|\beta_2|^2+R_1^*\langle\beta_1^*\beta_2\rangle+R_2^*\langle\beta_1\beta_2^*\rangle\}$$
$$-\nu\varepsilon^{1/2}\{|R_1-1|^2|\beta_1|^2+|R_2-1|^2|\beta_2|^2+2\,\mathrm{Re}[(R_1-1)(R_2-1)^*\langle\beta_1\beta_2^*\rangle]\}. \tag{40}$$

The terms proportional to $\nu\varepsilon^{1/2}$ are the negative definite collisional dissipation; the remaining terms are the correlation of $\langle n_k^*\phi_k\rangle$ written in terms of β_1 and β_2. The term $\mathrm{Im}\,R_1^*|\beta_1|^2$ is positive. If $\beta_2=0$, this term and the negative term $-\nu\varepsilon^{1/2}|R_1-1|^2|\beta_1|^2$ yield the linear growth rate $\mathrm{Im}\,\omega_1$. The term $\mathrm{Im}\,R_2^*|\beta_2|^2$ is negative. It and the term $-\nu\varepsilon^{1/2}|R_2-1|^2|\beta_2|^2$ yield the damping rate of the purely stable branch, $\mathrm{Im}\,\omega_2$. For nonlinear instability a necessary condition is $\mathrm{Im}\{R_1^*\langle\beta_1^*\beta_2\rangle+R_2^*\langle\beta_1\beta_2^*\rangle\}>0$. This condition can be rewritten as

$$\frac{k_y\nu_D}{\nu}\hat{\alpha}(1+k^2-\varepsilon^{1/2})\{\mathrm{Im}(\omega_1-\omega_2)\mathrm{Im}\langle\beta_1^*\beta_2\rangle$$
$$-[\mathrm{Re}(\omega_1-\omega_2)+O(\nu/k_y\nu_D)]\mathrm{Re}\langle\beta_1^*\beta_2\rangle\}>0. \tag{41}$$

The factors $\mathrm{Im}(\omega_1-\omega_2)$ and $\mathrm{Re}(\omega_1-\omega_2)$ are both positive. Thus, nonlinear instability is favored by having $\mathrm{Im}\langle\beta_1^*\beta_2\rangle>0$ and $\mathrm{Re}\langle\beta_1^*\beta_2\rangle<0$, although it could still occur for $\mathrm{Re}\langle\beta_1^*\beta_2\rangle>0$, provided the first term is sufficiently large. If the left-hand side of Eq. (41) is negative, or if its magnitude is smaller than the magnitude of negative terms in Eq. (40), the system has nonlinear damping. Both nonlinear damping and instability arise for different wave numbers in the energy input rate spectrum of Fig. 1. Nonlinear energy transfer to the damped branch assures that $\mathrm{Im}\langle\beta_1^*\beta_2\rangle>0$. (Recall that without the latter, there is no nonlinear eigenmode, and hence no nonlinear instability.) Thus, nonlinear instability is also favored by $\mathrm{Im}(\omega_1-\omega_2)>0$, and the disposition of linear eigenmode frequencies is seen to be a factor in nonlinear instability. The combination of growing and damped eigenmode branches makes $\mathrm{Im}(\omega_1-\omega_2)$ more positive than it would be if the second branch were weakly growing or marginally stable.

A necessary and sufficient condition for supercritical nonlinear instability is $\gamma_k^{nl}-\mathrm{Im}\,\omega_1>0$, or $\gamma_k^{nl}-\gamma_k^{nl}|_{\beta_2=0}>0$. Rewriting this expression in terms of $\mathrm{Re}\langle\beta_1^*\beta_2\rangle$ and $\mathrm{Im}\langle\beta_1^*\beta_2\rangle$, using the expression for R_1 and R_2 of Sec. II, and taking the saturation level scalings of Eq. (39) as a guide for an expansion in ν small, the instability condition becomes

$$\mathrm{Im}\langle\beta_1^*\beta_2\rangle\left[\frac{\hat{\alpha}(1+k^2)[3-\hat{\alpha}\varepsilon^{1/2}(2+\hat{\alpha}\varepsilon^{1/2})]-2-\hat{\alpha}\varepsilon^{1/2}(1-\hat{\alpha}\varepsilon^{1/2})}{(1-\varepsilon^{1/2}\hat{\alpha})}\right]$$
$$-\frac{(k_y\nu_D)}{\nu}\left\{\mathrm{Re}\langle\beta_1^*\beta_2\rangle\hat{\alpha}(1-\varepsilon^{1/2}\hat{\alpha})+|\beta_2|^2\left[\frac{(1-\hat{\alpha}\varepsilon^{1/2})[\hat{\alpha}(1+k^2)-\varepsilon^{1/2}+k^2]}{\varepsilon^{1/2}(1+k^2-\varepsilon^{1/2})}\right]\right\}>0. \tag{42}$$

It is evident that $\mathrm{Im}\langle\beta_1^*\beta_2\rangle>0$ tends to produce nonlinear instability. Because the same inequality is responsible for the transfer of energy from β_1 to β_2, the excitation of the damped eigenmode, and therefore the nonlinear eigenmode, is a nonlinearly destabilizing effect. On the other hand the damped eigenmode dissipates energy at finite amplitude, introducing the stabilizing term proportional to $|\beta_2|^2$. $\mathrm{Re}\langle\beta_1^*\beta_2\rangle>0$ is also stabilizing. Which terms are larger depends on the values of A_2, A_r, and A_i, which in turn depend on spectral details. The analysis of Sec. V A suggests that $A_r<A_i$, but the relative magnitudes of A_i and A_2 have not been determined. Because both stabilizing and destabilizing terms enter at lowest order, either stabilization or destabilization at finite amplitude is possible. Higher values of $\hat{\alpha}$ appear to favor nonlinear instability. The left-hand side (LHS) of Eq. (42) is evaluated in Figs. 1 and 6. For those parts of wave number space where γ_k^{nl} exceeds the linear growth rate, the LHS of Eq. (42) is positive, otherwise it is negative.

VI. DISCUSSION

The stabilization of linearly unstable modes at finite amplitude in some parts of the wave number spectrum and supercritical nonlinear instability in others is found to be a robust feature of the coupled dynamics of ion vorticity and electron density evolution under collisionless conditions. This type of behavior thus applies to systems like the Hasegawa–Wakatani equations and the trapped electron turbulence model studied here. The changes in the growth rate spectrum at finite amplitude arise from the advective nonlinearity. This nonlinearity excites fluctuation structures, or eigenmodes, that belong to the purely stable eigenmode branch and are often ignored. The nonlinear excitation of these linearly stable structures changes the relationship of density to potential dictated by the linear instability. This in turn changes the correlation of density and potential that controls free-energy extraction and instability. Nonlinear advection of scalar quantities like density, temperature, etc., is intrinsic to virtually all multifield models. Hence, the nonlinear instability mechanism studied here is fundamental. Other mechanisms associated with nonlinear instability, including those of self-trapping, magnetic shear, mode structure, and collisions, are not required. Nonlinear instability by this mechanism in models of ion temperature gradient turbulence is currently under study.

In this work we have studied supercritical nonlinear instability and finite amplitude-induced stabilization of linearly unstable modes. Subcritical nonlinear instability has not been examined. The behavior studied has important consequences. It leads to a saturation mechanism that differs from saturation regulated by a Kolmogorov-type cascade in wave number space. Under a Kolmogorov cascade, the turbulent steady state satisfies $\Sigma_k \gamma^l(k)\ E(k)=0$, which requires that the spectrum $E(k)$ evolve in shape until positive and negative ranges of the amplitude-independent linear growth rate $\gamma^l(k)$ are weighted equally in the spectrum-weighted sum. Under the two-field dynamics of Eqs. (1)–(2), $\gamma^l(k)$ is irrelevant at finite amplitude. Instead, the condition for steady state becomes $\Sigma_k \gamma^{nl}(k)\ E(k)=0$, where $\gamma^{nl}(k)$ is the energy input rate dictated by the amplitudes in the saturated state of the linearly unstable eigenmode and the nonlinearly excited, purely stable eigenmode. This condition is satisfied by both the finite-amplitude evolution of $E(k)$ and the evolution of the energy input rate from $\gamma^l(k)$ to $\gamma^{nl}(k)$.

The nonlinear evolution of the energy input rate means that spectral transfer within the unstable branch is typically weaker than it would be if $\gamma^l(k)$ were the energy input rate at finite amplitude. It also means that simple estimates of turbulence properties, like the mixing length rule for saturation level, and quasilinear expressions for transport fluxes, are flawed because of their reliance on $\gamma^l(k)$. The reduction of particle flux is interesting in the context of the particle pinch for collisionless plasmas.[26] For the part of the particle flux that is modeled as an outward diffusion we use the quasilinear flux, as is often done. The difference between the quasilinear flux and the true flux then takes the form of an inward pinch. While this part of the flux is smaller than the outward diffusion in the present model, it is only slightly smaller.

The difference between the true flux and the quasilinear flux is not as dramatic as the difference between $\gamma^{nl}(k)$ and $\gamma^l(k)$ because contributions to the flux from wave number regions where $\gamma^{nl}(k)>\gamma^l(k)$ and $\gamma^{nl}(k)<\gamma^l(k)$ partially cancel. One type of turbulence characterization that is directly sensitive to the difference between $\gamma^{nl}(k)$ and $\gamma^l(k)$, and is therefore likely to be strongly modified by the type of two-field dynamics described in this paper, is bispectral deconvolution analysis (BDA).[9] As presently formulated, BDA draws on the measurement of the bispectrum of a single fluctuating field. A generic one-field turbulence model is used to deconvolve the measured spectrum and infer the linear growth rate. This method has been applied to density fluctuation data measured by beam emission spectroscopy on the Tokamak Fusion Test Reactor (TFTR) device. The inferred growth rate is negative in an intermediate wave number region and positive at lower and higher wave numbers. The spectrum peak falls in the region of negative growth. Typically, spectral energies are repressed in regions of damping, unlike the results inferred in TFTR. This may reflect a nonlinear instability process with energy input and dissipation at different wave numbers than that of the linear growth rate. A multifield BDA algorithm is currently being developed to allow inference of linear and nonlinear growth rates from experimental data in such situations.[19]

ACKNOWLEDGMENTS

The authors acknowledge useful conversations with A. Rogister.

This work was supported by the US Department of Energy under Grant No. DE-FG02-89ER-53291.

APPENDIX: DERIVATION OF MODEL EQUATIONS

We trace briefly a simple derivation of Eqs. (1) and (2). We are interested in fluctuations whose scale is larger than the Debye length; hence quasineutrality holds, i.e., $n_i=n_e$, where n_i and n_e are the fluctuating ion and electron densities. Ion density satisfies a continuity equation

$$\frac{\partial n_i}{\partial t}+\mathbf{u}_i\cdot\nabla n_o(x)+\mathbf{u}_i\cdot\nabla n_i+n_o\nabla\cdot\mathbf{u}_i=0, \tag{A1}$$

where $n_o(x)$ is the mean density, $\mathbf{u}_i$ is the ion flow fluctuation, and the mean ion flow is assumed zero. The ion flow satisfies a momentum balance

$$\left(\frac{\partial\mathbf{u}_i}{\partial t}+\mathbf{u}_i\cdot\nabla\mathbf{u}_i\right)=\frac{e}{m_i}(\mathbf{E}+c^{-1}\mathbf{u}_i\times\mathbf{B})-(m_in_i)^{-1}\nabla p_i, \tag{A2}$$

where p_i is the ion pressure. For cold ions the pressure term is neglected, and the ion flow is solved perturbatively assuming that the fluctuation frequency ω is smaller than the frequency of ion gyration $\Omega=eB/m_ic$. The lowest-order solution yields the E×B drift $\mathbf{u}_i^{(0)}=\mathbf{u}_E=\mathbf{E}\times\mathbf{B}/B^2=-\nabla\ \phi\times z/B$, while the next order solution yields the polarization drift

$$\mathbf{u}_i^{(1)}=\frac{1}{\Omega_B}z\times\left(\frac{\partial}{\partial t}+\mathbf{u}_i^{(0)}\cdot\nabla\right)\mathbf{u}_i^{(0)}. \tag{A3}$$

Substituting $\mathbf{u}_i^{(0)}+\mathbf{u}_i^{(1)}$ into Eq. (A1) yields

$$\frac{\partial n_i}{\partial t}-\nabla\phi\times z\cdot\nabla n_i-\nabla^2\frac{\partial\phi}{\partial t}+\nabla\phi\times z\cdot\nabla\nabla^2\phi=-\nu_D\frac{\partial\phi}{\partial y}, \tag{A4}$$

where n_i and n_e are understood to be normalized by n_o. The last term comes from the advection of the mean density by $\mathbf{u}_E$, where $\nu_D=cT_e/eBL_n$, and $L_n=(d\ln n_o/dx)^{-1}$ is the density gradient scale length. The third and fourth terms come from the compression of the ion polarization drift $n_o\nabla\cdot\mathbf{u}_i=n_o\nabla\cdot\mathbf{u}_i^{(1)}$. The E×B drift is incompressible if the magnetic field is homogeneous. Particle trapping, of course, implies an inhomogeneous magnetic field, for which $\nabla\cdot\mathbf{u}_E$ gives rise to curvature terms.[27] Curvature terms are small if $a\nabla>\Omega/\omega$, which requires $L_na^{-1}<k_y^2\rho_s^2$, where a is the minor radius. This approximation can break down at long wavelengths and in the core of tokamaks, where L_na^{-1} is not very small. In keeping with our general philosophy of examining nonlinear instability in the simplest of systems, we neglect curvature effects, just as we have neglected magnetic shear. Both effects are worth considering in future studies. Contributions from $\mathbf{u}_i^{(1)}$ in the advective terms are small compared to the terms retained in Eq. (A4). The relative magnitude of terms retained to those neglected is detailed in Ref. 28.

The electron density is given by the sum of a Boltzmann response and a nonadiabatic correction representing the density of trapped electrons, $n_e=\phi+\varepsilon^{1/2}\hat{n}_e$. The nonadiabatic electron density $\hat{n}_e$ is governed by electron continuity, with flow as the E×B drift

$$\frac{\partial\hat{n}_e}{\partial t}-\nabla\phi\times z\cdot\nabla\hat{n}_e+\upsilon\hat{n}_e=-\frac{\partial\phi}{\partial t}-\nu_D(1+\alpha\eta_e)\frac{\partial\phi}{\partial y}. \tag{A5}$$

The last term arises from the advection of equilibrium gradients by the E×B flow and includes a temperature gradient term $\alpha\eta_e$, where $\alpha=3/2$. With the quasineutrality condition $n_i=\phi+\varepsilon^{1/2}\hat{n}_e$, Eqs. (A4) and (A5) form a closed system for n_i, $\hat{n}_e$, and ϕ. Quasineutrality can be used to eliminate n_i. Introducing a modified electron density $n=\varepsilon^{-1/2}n_e+\phi$ yields Eqs. (1) and (2). The choice of a trapped-electron regime for the nonadiabatic electron density implies the usual condition on collisionality, i.e., the bounce frequency must exceed the collisional detrapping frequency υ. In auxiliary heated tokamaks all of the plasma typically falls in this regime except the extreme edge and scrape-off layer. Within the trapped electron regime there is a collisional and collisionless regime according to $\upsilon\gtrless k_y\nu_D$. In TEXT, the outer part of the trapping regime was collisional, while the collisional limit extended inward from the radius where $T_e=0.6$ keV.[26] In TFTR significant auxiliary power pushed the collisional regime to the edge of the plasma, putting most of the plasma in the collisionless regime. Collisionless trapped electron dynamics is thus highly relevant. However, it should be emphasized that the representation of trapped electron physics in Eqs. (1) and (2) is both simplified and approximate to a considerable degree.

[1] R. H. Berman, D. J. Tetreault, T. H. Dupree, and T. Boutros-Ghali, Phys. Rev. Lett. **48**, 1249 (1982).
[2] P. W. Terry, P. H. Diamond, and T. S. Hahm, Phys. Fluids B **2**, 2048 (1990).
[3] S. Hirshman and K. Molvig, Phys. Rev. Lett. **42**, 648 (1979).
[4] D. Biskamp and A. Zeiler, Phys. Rev. Lett. **74**, 706 (1995).
[5] J. F. Drake, A. Zeiler, and D. Biskamp, Phys. Rev. Lett. **75**, 4222 (1995).
[6] B. D. Scott, Phys. Rev. Lett. **65**, 3289 (1990).
[7] R. V. Bravenec, D. W. Ross, P. M. Schoch, D. L. Brower, J. W. Heard, R. L. Hickok, P. W. Terry, A. J. Wootton, and X. Yang, Nucl. Fusion **31**, 687 (1991).
[8] K. Burrell, Phys. Plasmas **4**, 1499 (1997).
[9] J. S. Kim, R. J. Fonck, R. D. Durst, E. Fernandez, P. W. Terry, S. F. Paul, and M. C. Zarnstorff, Phys. Rev. Lett. **79**, 841 (1997).
[10] D. A. Baver, P. W. Terry, and E. Fernandez, Phys. Lett. A **267**, 188 (2000).
[11] A. Hasegawa and M. Wakatani, Phys. Rev. Lett. **50**, 682 (1983).
[12] K. Itoh, S.-I. Itoh, and A. Fukuyama, *Transport and Structural Formation in Plasmas* (Institute of Physics, Bristol, 1999).
[13] L. Garcia, B. A. Carreras, and P. H. Diamond, Phys. Fluids **30**, 1388 (1987).
[14] N. Mattor and P. H. Diamond, Phys. Fluids **31**, 1180 (1988).
[15] D. E. Newman, P. W. Terry, P. H. Diamond, Y.-M. Liang, G. G. Craddock, A. E. Koniges, and J. A. Crotinger, Phys. Plasmas **1**, 1592 (1994).
[16] P. W. Terry, D. E. Newman, and A. S. Ware, Phys. Plasmas **1**, 3974 (1994).
[17] G. G. Craddock, A. E. Koniges, J. A. Crotinger, P. H. Diamond, D. E. Newman, and P. W. Terry, Phys. Plasmas **1**, 1877 (1994).
[18] D. R. Demers, P. M. Schoch, T. P. Growley, K. A. Connor, and A. Ouroua, Phys. Plasmas **8**, 1278 (2001).
[19] D. A. Baver and P. W. Terry, Bull. Am. Phys. Soc. **45**, 336 (2000).
[20] Z. Lin, T. S. Hahm, W. W. Lee, W. M. Tang, and P. H. Diamond, Phys. Rev. Lett. **83**, 3645 (1999).
[21] G. R. Tynan, R. A. Moyer, M. J. Burin, and C. Holland, Phys. Plasmas **8**, 2691 (2001).
[22] R. Gatto, P. W. Terry, and D. A. Baver, Bull. Am. Phys. Soc. **46**, 164 (2001).
[23] A. E. Koniges, J. A. Crotinger, and P. H. Diamond, Phys. Fluids B **4**, 2785 (1992).
[24] D. E. Newman, P. W. Terry, P. H. Diamond, and Y.-M. Liang, Phys. Fluids B **5**, 1140 (1993).
[25] F. Y. Gang, P. H. Diamond, J. A. Crotinger, and A. E. Koniges, Phys. Fluids B **3**, 955 (1991).
[26] P. W. Terry, Phys. Fluids B **1**, 1932 (1989).
[27] R. E. Waltz, Phys. Fluids **28**, 577 (1985).
[28] P. W. Terry and W. Horton, Phys. Fluids **25**, 491 (1982).